The Impact of Energetic Particles on the Martian Ionosphere During a Full Solar Cycle of Radar Observations: Radar Blackouts

Mark Lester, Beatriz Sanchez-Cano, Daniel Potts, Rob Lillis, Marco Cartacci, Fabrizio Bernardini, Roberto Orosei, Matthew Perry, Nathaniel Putzig, Bruce Campbell, et al.

The Impact of Energetic Particles on the Martian Ionosphere During a Full Solar Cycle of Radar Observations: Radar Blackouts

Mark Lester[1] [ID], Beatriz Sanchez-Cano[1] [ID], Daniel Potts[1] [ID], Rob Lillis[2] [ID], Marco Cartacci[3], Fabrizio Bernardini[3], Roberto Orosei[4] [ID], Matthew Perry[5] [ID], Nathaniel Putzig[5] [ID], Bruce Campbell[6] [ID], Pierre-Louis Blelly[7] [ID], Steve Milan[1] [ID], Hermann Opgenoorth[8,1], Olivier Witasse[9] [ID], Elena M. M. Redrojo[10] [ID], and Aaron Russell[5]

[1]School of Physics and Astronomy, University of Leicester, Leicester, UK, [2]Space Sciences Laboratory, University of California, Berkeley, CA, USA, [3]Istituto di Astrofisica e Planetologia Spaziali, Istituto Nazionale di Astrofisica, Rome, Italy, [4]Istituto di Radioastronomia, Istituto Nazionale di Astrofisica, Bologna, Italy, [5]Planetary Science Institute, Lakewood, CO, USA, [6]Center for Earth and Planetary Studies, Smithsonian Institution, Washington, DC, USA, [7]Institut de Recherche en Astrophysique et Planétologie, Toulouse, France, [8]Umeå University, Umea, Sweden, [9]European Space Agency (ESA), European Space Research and Technology Centre (ESTEC), Noordwijk, The Netherlands, [10]Valquer Laboratorios, Villaminaya, Spain

Abstract We present the first long-term characterization of ionization layers in the lower ionosphere of Mars (below ~90 km), a region inaccessible to orbital in-situ observations, based on an analysis of radar echo blackouts observed on Mars Express and the Mars Reconnaissance Orbiter from 2006 to 2017. A blackout occurs when the expected surface reflection is partly or totally attenuated for portions of an observation. Enhanced ionization at altitudes of 60–90 km, below the main ionospheric electron density peak, leads to increased absorption of the radar signal, resulting in the blackouts. We find that (a) MARSIS, operating at frequencies between 1.8 and 5 MHz, suffered more blackouts than SHARAD, which has a higher carrier frequency (20 MHz), (b) there is a clear correlation of blackout occurrence with solar cycle, (c) there is no apparent relationship between blackout occurrence and crustal magnetic fields, and (d) blackouts occur during both nightside and dayside observations, although the peak occurrence is deep on the nightside. Analysis of Mars Atmosphere and Volatile EvolutioN Solar Energetic Particle electron counts between 20 and 200 keV demonstrates that these electrons are likely responsible for attenuating the radar signals. We investigate the minimum SEP electron fluxes required to ionize the lower atmosphere and produce measurable attenuation. When both radars experience a blackout, the SEP electron fluxes are at their highest. Based on several case studies, we find that the average SEP spectrum responsible for a blackout is particularly enhanced at its higher energy end, that is, above 70 keV.

Plain Language Summary The orbital radars that study the surface and subsurface of Mars can suffer a near-total loss of received signal during periods when high-energy electrons from the Sun enter the Martian atmosphere, causing enhanced ionization at altitudes between 60 and 90 km. We have studied these radar blackouts using radars on the Mars Express and Mars Reconnaissance Orbiter spacecraft. The radars on the two spacecraft work at different frequencies, allowing us to test the theory that a larger effect is predicted at lower frequency. Indeed, we do see more blackouts of the radar operating at lower frequency (1.8–5 MHz) than at the higher frequency (20 MHz). We also find that more blackouts occur for both radars during periods of higher solar activity that is, more solar flares and Coronal Mass Ejections. The radar blackouts occur on the nightside and dayside and over all locations on the planet's surface, indicating a global effect of the solar particle events. We have also investigated the electron fluxes measured by the Mars Atmosphere and Volatile EvolutioN spacecraft and find they are higher during blackouts that include the 20 MHz frequency. These observations provide a new window on the levels of ionization at low altitudes.

1. Introduction

The last two decades have witnessed a considerable expansion of our knowledge of Mars, its surface, atmosphere and plasma environment, as well as how these different parts of the Martian system interact. Observations have been made with orbiting spacecraft as well as a series of landers and rovers, making both in situ and remote

sensing measurements. The orbiting spacecraft, Mars Express (MEx; Chicarro et al., 2004) and Mars Reconnaissance Orbiter (MRO; Zurek & Smrekar, 2007), carry sounding radars (MARSIS, the Mars Advanced Radar for Subsurface and Ionosphere Sounding on MEx, and SHARAD, the Shallow Radar on MRO) that probe the Martian ionosphere, surface, and the upper layers of the crust at frequencies between 1.5 and 25 MHz. For surface and subsurface sounding, the radar signals must pass through the ionosphere. While that passage may distort echoes from the surface and subsurface, it can also be beneficial scientifically for other studies, as the resultant time delay of the signal passing through the ionized medium can be used to derive the ionospheric Total Electron Content, TEC (e.g., Campbell et al., 2011; Campbell & Watters, 2016; Cartacci et al., 2018, 2013; Conroy et al., 2020; Safaeinili et al., 2007; Sanchez-Cano et al., 2015). However, the data may be of little use for either purpose if enhanced ionization at low altitude results in increased attenuation such that the power of the returned signal is reduced below the background noise level (Campbell et al., 2014; Espley et al., 2007; Morgan et al., 2006). Such occurrences are particularly problematic if the enhanced ionization occurs below 100 km since attenuation due to electron-neutral collisions is most effective at relatively high neutral densities. Events such as these are termed "radar blackouts" and typically occur during major space weather events (e.g., Sanchez-Cano et al., 2019). The distribution of ionization at altitudes below 100 km is not well understood as it is not accessible to in situ measurements by orbiters and, so far, there have been no instruments such as riometers or ionosondes on landed spacecraft that can probe this region remotely. The need for data in this region has grown, since it is now apparent that the coupling between the lower atmosphere and the upper atmosphere at Mars is particularly important for understanding both the history of the planet's atmosphere and its current behavior (e.g., Chaffin et al., 2018; Jakosky et al., 2018). Sanchez-Cano et al. (2019) studied a radar blackout that occurred for 10 days on MARSIS and 3 days on SHARAD. Comparison with simultaneous observations by the Solar Energetic Particle (SEP) instrument on MAVEN indicated that electrons in the energy range 20–200 keV were responsible. Modeling of the impact of these electrons demonstrated the additional ionization created below 100 km and the subsequent absorption profile for both radars was sufficient to cause both radars to be unable to receive a signal from the ground. Although this paper sheds some light on the nature of the particles, which might cause enhanced ionization layers, further detailed study is required.

Attenuation is one of four major effects of the passage of radar signals through planetary ionospheres (e.g., Campbell et al., 2014; Safaeinilli et al., 2003). Others include an increased time delay, distortion of the signal phase, and Faraday rotation (if the magnetic fields are sufficiently intense). At Mars, we note that the impact of the magnetic field is likely to be small, due to the low field strength compared with Earth (e.g., Nielsen et al., 2007). Following the formulation of Sanchez-Cano et al. (2019), the variation of the attenuation, A (in dB/m), as a function of height, h, above the planet's surface, of a radio signal propagating through an ionized medium is given by:

$$A(h) = 4.61 \times 10^{-7} N_e(h) \frac{\nu(h)}{(2\pi f)^2 + \nu^2(h)}, \qquad (1)$$

where N_e is the electron density in m^{-3}, ν is the momentum-transfer electron-neutral collision frequency in Hz, and f is the frequency in Hz of the radio wave. At Mars, the main neutral species in the lower ionosphere is expected to be carbon dioxide, CO_2 (Montmessin et al., 2017, and references therein). The electron-neutral collision frequency is proportional to the neutral density, which increases exponentially as the altitude decreases, and hence Witasse et al. (2001) demonstrated that the absorption caused by even a relatively low-density electron layer in the lower atmosphere would result in more attenuation than in the main ionosphere layer, where the electron density reaches a maximum. Further theoretical work on the level of absorption at all levels of the Martian atmosphere confirmed that additional ionization at altitudes below the two main peaks in the Martian ionosphere could result in the total absorption of the radar ground signal (Withers, 2011). Sheel et al. (2012) modeled the impact of protons of energies greater than 1 MeV during a major solar energetic proton event observed at Earth to demonstrate that such ions could create additional ionization. Sanchez-Cano et al. (2019), however, demonstrated the impact of the SEP electron fluxes, as well as noting that the peak attenuation occurred at the altitude where the radar operating frequency equaled the electron-neutral (CO_2) collision frequency. Thus, at this altitude even a small N_e will result in significant absorption. The attenuation is inversely proportional to the radio frequency, so Equation 1 predicts that attenuation is lower for higher frequencies. As the SHARAD operating frequency (20 MHz) is a factor of about five higher than the MARSIS operating frequency (1.8–5 MHz), data from these instruments provide a means to test this prediction.

In this study, our aim is to examine the relationship between solar particle events and the radar blackouts seen by SHARAD and MARSIS over the interval 2006–2017, effectively a whole solar cycle. The main goal is to investigate under which conditions such radio-absorbing ionization is found in the lower ionosphere of Mars during different portions of a solar cycle. This study provides the first long-term characterization of the lower ionosphere of Mars, a region inaccessible to other types of orbiter observations. Taking advantage of the long period of operation by MARSIS and SHARAD, we present a statistical analysis of the occurrence frequency of the blackouts experienced by the two radars as well as studying their correlation with respect to Mars' crustal magnetic fields. The work is supported by four case studies, which look at the effects of enhancements in SEP electrons, allowing us to investigate the energy-flux spectra of the particles responsible for the complete and partial blackouts measured by the radars. Three case studies look at individual events, while the fourth has two separate enhancements in SEP particles. All case studies are taken from the 2014 to 2017 interval when data from the Mars Atmosphere and Volatile EvolutioN (MAVEN) mission (Jakosky et al., 2015) are available during the longer period of interest for SHARAD and MARSIS mentioned above.

2. Data Sets and Selection

This study uses data from the subsurface sounding mode of the MARSIS instrument (Orosei et al., 2015; Picardi et al., 2004) on MEx, and from the SHARAD sounder (Campbell et al., 2011; Seu et al., 2004) on MRO to identify times when there is either a total or a partial blackout of the radar signal. In addition, data taken from the SEP instrument on MAVEN provide the energy-flux spectra of high energy particles (ions and electrons) during the blackouts. We also present data from the Extreme Ultra Violet Monitor (EUVM) on MAVEN to provide context for the high energy particle observations.

Here we give a brief description of each instrument and the nature of its data. MARSIS operates in two distinct experimental modes, the so-called SubSurface mode and the Active Ionospheric Sounding (AIS) mode. This study focuses only on the SubSurface mode, where the radar alternates the transmission at two different frequencies, choosing from 1.8, 3, 4 and 5 MHz, to investigate the nature of the surface and subsurface. The two frequencies are selected to be higher than the ionospheric peak plasma frequency (Orosei et al., 2015) so they can propagate through the ionosphere. In this study, we select data where the MARSIS lower frequency used on the nightside is typically 1.8–3 MHz, and 4–5 MHz on the dayside, depending upon the planned operations. The MARSIS SubSurface mode typically operates for 15 min either side of the spacecraft periapsis, which has varied from 275 to 350 km during the mission, a limited portion of the seven-hour orbital period (e.g., Stergiopoulou et al., 2020). Further, the radar is not operated on every orbit to accommodate the operation of other instruments. There are also times when the radar is not operated due to spacecraft constraints, such as periods of eclipse when the available power is insufficient.

In the subsurface mode, MARSIS transmits pulses at the two frequencies on independent channels, and records received power as a function of the time delay of the signal return, producing a display referred to as a radargram. To remove the ionospheric phase distortion that affects the MARSIS signals, the data are processed using a dedicated algorithm, the so-called Contrast Method (CM; Cartacci et al., 2013). The CM algorithm consists of a loop, where the range compression of the radar signal is iterated with different correction phases until the signal is optimally compressed. The noise level for MARSIS is determined mainly by galactic noise, which is of order 35 dB at 4 MHz and 25 dB at 5 MHz. The performance of the CM can vary according to ionospheric conditions. Considering the higher MARSIS frequencies (4–5 MHz), the CM parameters are set to work reliably for SZA larger than ~60°–70°, while for lower values of SZA, the attenuation starts to considerably reduce the signal reliability. For this reason, as well as the observation of Espley et al. (2007) that the loss of the surface signal can be due to daytime ionization at the normal electron density peak, we considered only data with SZA>50° in this study. In case of high solar activity, both attenuation and phase distortion can be so heavy that a correct range compression is very difficult to obtain even through the CM. When this happens, the signal is characterized by a Signal to Noise Ratio (SNR) that is very low (partial blackout) or even below the noise level (total blackout).

Examples from March 2014 of the received signal during a normal pass, a total blackout, and a partial blackout are given in Figure 1a, from left to right, respectively. Each panel presents a radargram, which displays the received signal power as a function of time delay (y-axis) and of the position along the orbital track (x-axis) for the highest transmitted frequency. The surface is seen in the left panel of Figure 1a as a strong returned signal at
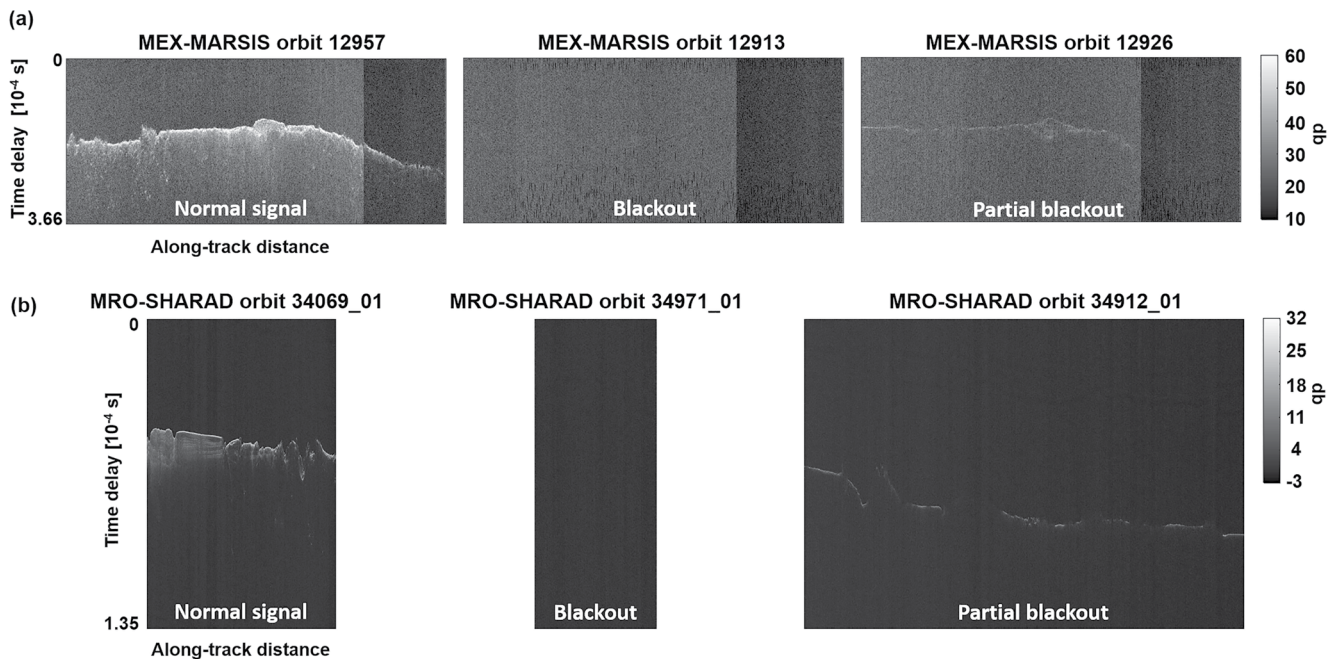
Figure 1. Examples of the radar signals received by MARSIS (Figure 1a) and SHARAD Figure (1b). The radar's received signal strength is plotted as a function of time delay and the along track distance (Note the different scales for signal strength at the two satellites). The left-hand panels are examples of a normal returned signal, the central panels are examples of the radar signal during a total blackout, and the right hand panels of a partial blackout. SHARAD radargrams come from the US Planetary Data System products.

an uncalibrated echo power of about 50 dB. The irregular nature of this returned signal is a result of the planet's topography together with the delay introduced by the ionosphere, while the dispersion in delay is mainly due to clutter. This clutter results from surface backscattering coming from the cross-track direction, and, in the second half of the left panel, by the signal returned from the subsurface. The abrupt change in the noise background and the change in nature of the surface signal toward the end of the radargram is a result of the increase in the operating frequency from 4 to 5 MHz that normally occurs around SZA<90°. The lack of any clearly returned signal during a blackout is illustrated in the central panel of Figure 1a. There is no evidence for a ground return in the entire radargram. The received signals are all at a similar level to the background noise signal, although this noise signal level again changes as a result of the operational frequency shift. An example of a partial blackout, in the right hand panel of Figures 1a, is illustrated by the much weaker clutter and returned signal, with only an occasional surface signal at a similar level to that in the left hand panel of Figure 1a. The surface signal disappears just before the operational frequency increase and does not appear again even at the frequency of 5 MHz. Note that we take no account here of the potential heterogeneity of the surface in the loss of the received signal in the last two examples.

SHARAD operates at a higher center frequency of 20 MHz with a 10 MHz bandwidth, and MRO is in a sun-synchronous orbit (15:00 local time ascending node), the altitude of which varies between 250 and 320 km. Thus, the radar is able to make observations for a larger part of each orbit than MARSIS and has operated for a much greater fraction of the period under study. A sharpness metric maximizes the power of the radar signal to produce the phase correction. This is applied to the signal to unwrap the dispersion effects of the ionosphere across the bandwidth, thereby providing the SHARAD ionospheric correction (Campbell et al., 2014). The phase correction is also used to determine the range delay position. The noise level for SHARAD is determined by the galactic noise as well as spacecraft noise. After range compression, the surface signal is, under normal circumstances, of order 29 dB above the noise floor. In this study, the timings and SHARAD plots come from the SHARAD US Reduced Data Record (RDR) data products that do not take into account any approximate attenuation as a function of TEC, nor any correction due to lower atmosphere effects. Examples of SHARAD radargrams from an unaffected orbit segment, one with a total blackout, and one with a partial blackout are given in the panels of Figure 1b from left to right, respectively. The normal orbit is taken from November 2013, while the other two in Figure 1b are from January 2014. The format of the panels is the same as for the MARSIS examples, although the

signal strength scale is different. In a similar fashion to the MARSIS data, the unaffected radargram (Figure 1b, left hand panel) has a very clear surface echo, while the total blackout effect is also very clear (Figure 1b, central panel). The partial blackout (Figure 1b, right hand panel) is marked by a reduced or fully attenuated signal. We note that several radargrams have black narrow stripes caused by technical issues, such as telecommunications issues that prevented ground recovery of the full data set for the observation. These cases are not considered as blackouts. However, there are a few cases with no-data stripes that are identified as partial blackouts, since the reason behind the partial loss of signal is operational rather than physical.

The Solar Energetic Particle (SEP) instrument on the MAVEN spacecraft (Larson et al., 2015) measures incident electrons and ions in the energy ranges 20–200 keV and 20 keV to 6 MeV, respectively, although the instrument can be susceptible to higher energy protons. The instrument consists of two sensors orthogonally mounted, each consisting of a pair of double-ended telescopes sensitive to primarily electrons at one end and ions on the other, covering ∼12% of the total sky. Here we follow the example of Sanchez-Cano et al., (2019) in using data only from the Forward 1 (F1) look direction, although we note that all telescopes observe very similar energy distributions during the events under study due to the electrons' relative isotropy. Finally, the Extreme Ultra Violet Monitor (EUVM) on MAVEN (Eparvier et al., 2015) provides a measurement of solar extreme ultraviolet and X-ray irradiance in three wavelength bands using three separate radiometers. One band is centered on the Lyman-α wavelength at 121.6 nm, while the other two channels cover the wavelength ranges 0.1–7 nm and 17–22 nm, providing information on different parts of the solar spectrum. Here we focus on the 0.1–7 nm band (Channel B), which is most sensitive to solar flares.

3. Statistics of Radar Blackouts

In this section, we consider the statistics of the occurrence of the radar blackouts in MARSIS and SHARAD observations. We focus on the interval 2006–2017, which starts in the declining phase of cycle 23, includes the somewhat extended minimum between solar cycles 23 and 24, and goes past the peak of cycle 24. We have identified the events by eye rather than try developing an automated algorithm. This involves sorting through the full data set for each radar for the entire interval. This has been done by multiple authors to ensure that we have a consistency of approach. At least two authors identified the blackouts independently, and another provided an independent list of events at SHARAD which confirmed the original identification. A total blackout was identified if there was no trace of the surface signal in a radargram representing a single orbit (see central panels of Figures 1a and 1b). The approach is inevitably slightly more subjective for partial blackouts. If there was no surface signal for part of the orbit as indicated by the radargram, then this was considered as a partial blackout. In addition a partial blackout would also be identified if the radargram demonstrated no clutter and/or a much weaker surface signal than would normally be expected (see right hand panels of Figures 1a and 1b). We have excluded any events where the loss of signal may have been due to a technical issue with the instrument or data transmission. A full list of blackouts is available at Lester and Sanchez-Cano (2021). We provide a description of when the blackouts occur, an overview of where they occur in relation to the planetary surface, the relationship between blackout occurrence and SZA, and finally the variation of the blackouts with respect to the solar cycle.

3.1. Overview of When Radar Blackouts Occur

Figure 2 presents the occurrence of the radar blackouts for MARSIS (left hand panels) and SHARAD (right hand panels). Each panel represents one year of the interval, starting with 2006 at the top and increasing downward. A gray vertical line in the panels indicates that the respective subsurface radar was operational with no technical issues and receiving a ground signal. We identify the orbits where a full radar blackout occurred by the vertical red lines, while orbits where a partial blackout was identified are plotted as blue vertical lines. There are many more orbits where SHARAD was operational compared with MARSIS. In addition, extended periods and shorter irregular periods exist where each radar was not in operation. In the case of MARSIS, there are periods when the spacecraft was in eclipse and, to conserve power, the radar was not in operation. These stand-down periods occur at the end of 2008, start of 2011, April 2013, and then the summer months of 2015 and 2017. Moreover, there are other periods with no operations every 26 months when superior conjunctions occur between Earth and Mars. The shorter periods are typically related to the operational requirements of the mission. Mars orbit insertion of MRO occurred on the 10 March 2006 and was followed by a 6-month aerobraking phase. The SHARAD data set used here begins in December 2006. The largest extended period when SHARAD was not operated, in
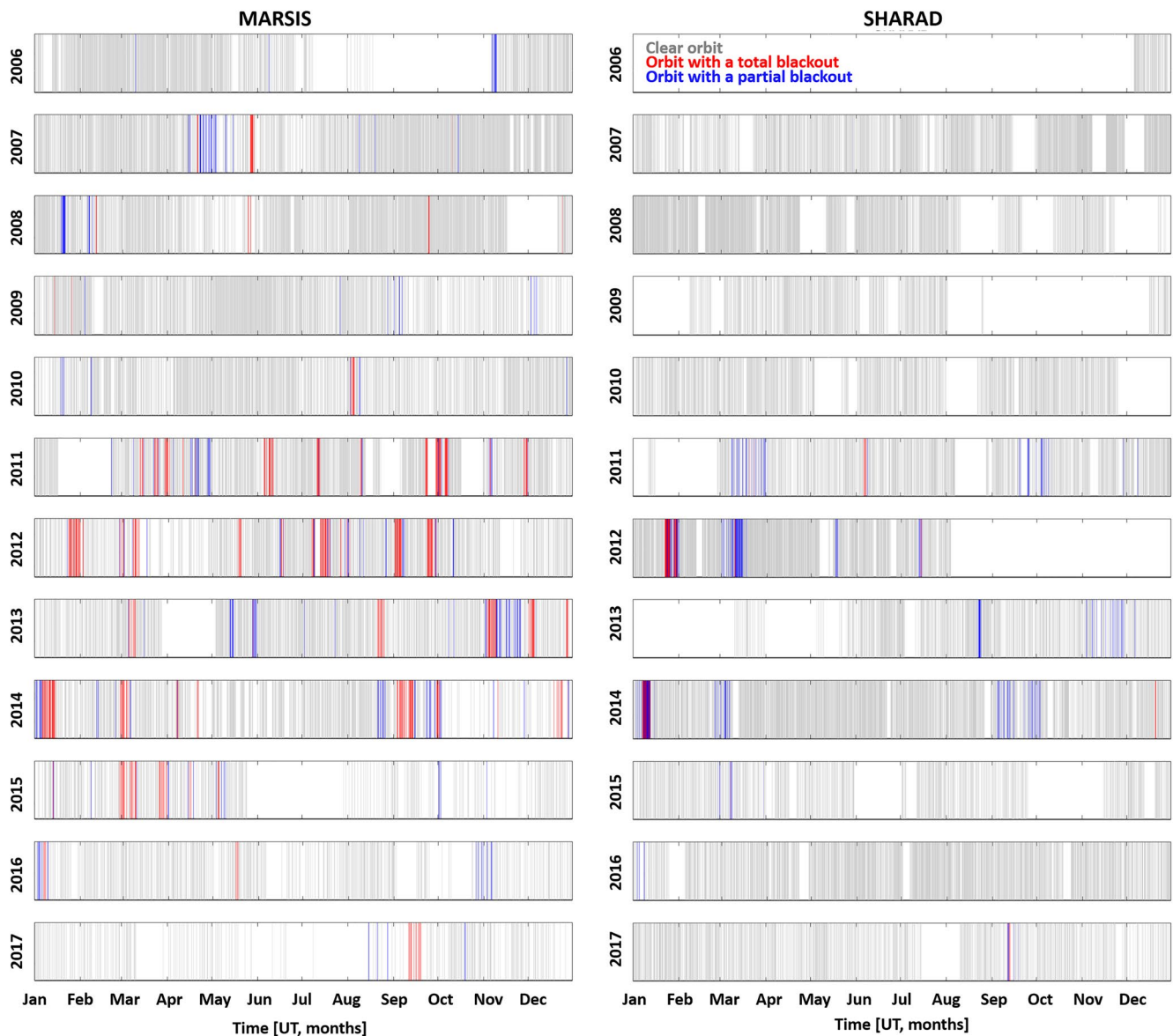
Figure 2. The orbits where the subsurface radar is operating (gray vertical line), where a total blackout occurs (red vertical line) and a partial blackout occurs (blue vertical line). The left hand panels are for MARSIS and the right hand panels for SHARAD. Each row represents one calendar year starting from 2006 at the top.

2012–2013, was due to changes in the management and support of the instrument operations. Over our study period, there are 7,697 MEx orbits and 20,785 MRO orbits when each radar was operated, representing the sum of the gray, red and blue lines in Figure 2 for each spacecraft.

Figure 2 illustrates a number of features regarding radar blackouts. First, there are more orbits where the MARSIS radar suffered a blackout than there are for SHARAD. There are 602 MARSIS orbits where there was a total or partial blackout whereas there are only 377 similar SHARAD orbits, representing 7.8% of MARSIS orbits and 1.8% of SHARAD orbits. We can also estimate the extent of time that the radar was blacked out, recognizing that due to the lack of continuous observations, this is only an approximate estimate. The length of the orbit is defined from the start time of the first orbit where a total or partial blackout occurs to the end time of the orbit where a total or partial blackout occurs. Only periods where there is a continuous run of orbits is considered. For MARSIS the average length of a blackout period is just over 8 days. The longest periods, both of order 15 days, were seen in November 2013 and December 2013 to January 2014. In January 2012 and September 2014 blackout periods

of about 12 days occurred. The average length of the radar blackouts at SHARAD was just under 3 days with the longest period in January 2012 of 10 days.

As confirmation of our identification of the blackout events for this study, we note that a number of these events have already formed the basis of previous case studies. Prior to the arrival of MAVEN at Mars these include the event in June 2011 where the surface reflected signal was not received during both AIS and subsurface modes (Morgan et al., 2014). Further, the High Energy Neutron Detector (HEND) on Mars Odyssey indicated the presence of solar energetic particles during the passage of an Interplanetary Coronal Mass Ejection (ICME) in June 2011. The subsurface signal on SHARAD was also lost during this event. In March and April 2012 a visible "plume" separating from the Martian disk was observed by the Hubble space telescope (Sanchez-Lavega et al., 2015) and the plasma conditions during this interval have been discussed by Andrews et al. (2016). These authors noted that during one of the intervals of plume observations, on 13 March 2012, the surface reflection was not present in the AIS ionogram (their Figure 3g). This interval corresponds to a total blackout of MARSIS and a partial blackout of SHARAD. Following the arrival of MAVEN, Jakosky et al. (2015) discussed the interaction of an ICME at Mars in March 2015, which is our Case Study 3 (see Section 4.3). This event is characterized by mainly total blackouts at MARSIS and partial blackouts at SHARAD. Also, the event in September 2017 discussed by Sanchez-Cano et al. (2019) initiated this study and is our Case Study 1 (see Section 4.1).

By contrast, during a period in August–November 2016 there were four separate Corotating Interaction Regions (CIR), each of which resulted in enhanced SEP electron fluxes and in either reduction or a total blackout of the AIS 4 MHz signal (Krishnaprasad et al., 2020). The first and third of these events may also have been coincident with an ICME. A weakening of the surface signal observed by AIS occurred on 7 August 2016 at the time of enhanced SEP electron fluxes. Two events on 4 and 29 September 2016 resulted in a weak signal and a total blackout of AIS data. However, the SubSurface mode was rarely operational during this time (Figure 2). The last of the enhancements in SEP electron fluxes on 24 October 2016 was close to some partial blackouts of the subsurface MARSIS mode. SHARAD recorded no blackouts during any of these events. Another space weather event in March 2008 associated with a weak ICME during solar minimum produced no evidence for a radar blackout in either mode of the MARSIS signal (Sanchez-Cano et al., 2017). Our study likewise does not find any blackout at this time (Figure 2), although there is no evidence for any SEP events during this event. Similarly, Opgenoorth et al. (2013) discussed events during solar minimum and just before the start of the next solar cycle, in March and April 2010. The interval of interest consisted of two CIR events and one ICME, in April 2010. Only AIS data were discussed in this paper but there was no evidence for a radar blackout during the ICME (Figure 2) and again no evidence for any SEP event, although the average energy of the magnetosheath electrons was noted as being generally higher during this period.

3.2. Overview of Where Radar Blackouts Occur

In Figure 3a we present the occurrence of the radar blackouts (full and partial) as a function of geographic location. We do not consider the SHARAD blackouts, as their occurrence frequency is much smaller than for MARSIS. MARSIS makes a series of radar soundings during each orbit and the latitude and longitude of each of these soundings is used in producing Figure 3. The data are plotted in planetocentric IAU reference frame coordinates in bins of $10°$ in latitude and longitude. The data have been divided into observations that occur on the dayside, where the spacecraft X co-ordinate in Mars centered Solar Orbital (MSO) co-ordinates, X_{MSO}, was positive, and those that occur on the nightside, that is, $X_{MSO} < 0$ (right hand panels). We choose only intervals where the SZA angle was greater than $50°$. The observations suggest that, in general, radar blackouts occur more or less at all longitudes and latitudes, and they occur at least as often on the nightside as on the dayside. There does appear to be some geographical variability from dayside to nightside, however, with more events occurring in mid- and equatorial latitudes on the dayside and more events in the polar regions on the nightside.

To remove any bias due to orbit coverage, Figure 3b presents the occurrence of the MARSIS operations plotted in the same co-ordinate system. Here we note that for the dayside (left hand panel) the distribution of coverage tends to peak in the polar regions of both hemispheres, while for the nightside, there are more observations in the southern hemisphere. There are over twice the number of orbits over the nightside than the dayside. The normalized occurrence is then presented in Figure 3c. Here we see that the occurrence frequency of radar blackouts on the dayside does appear to peak at mid- and equatorial latitudes, with a clear minimum at polar latitudes. On the
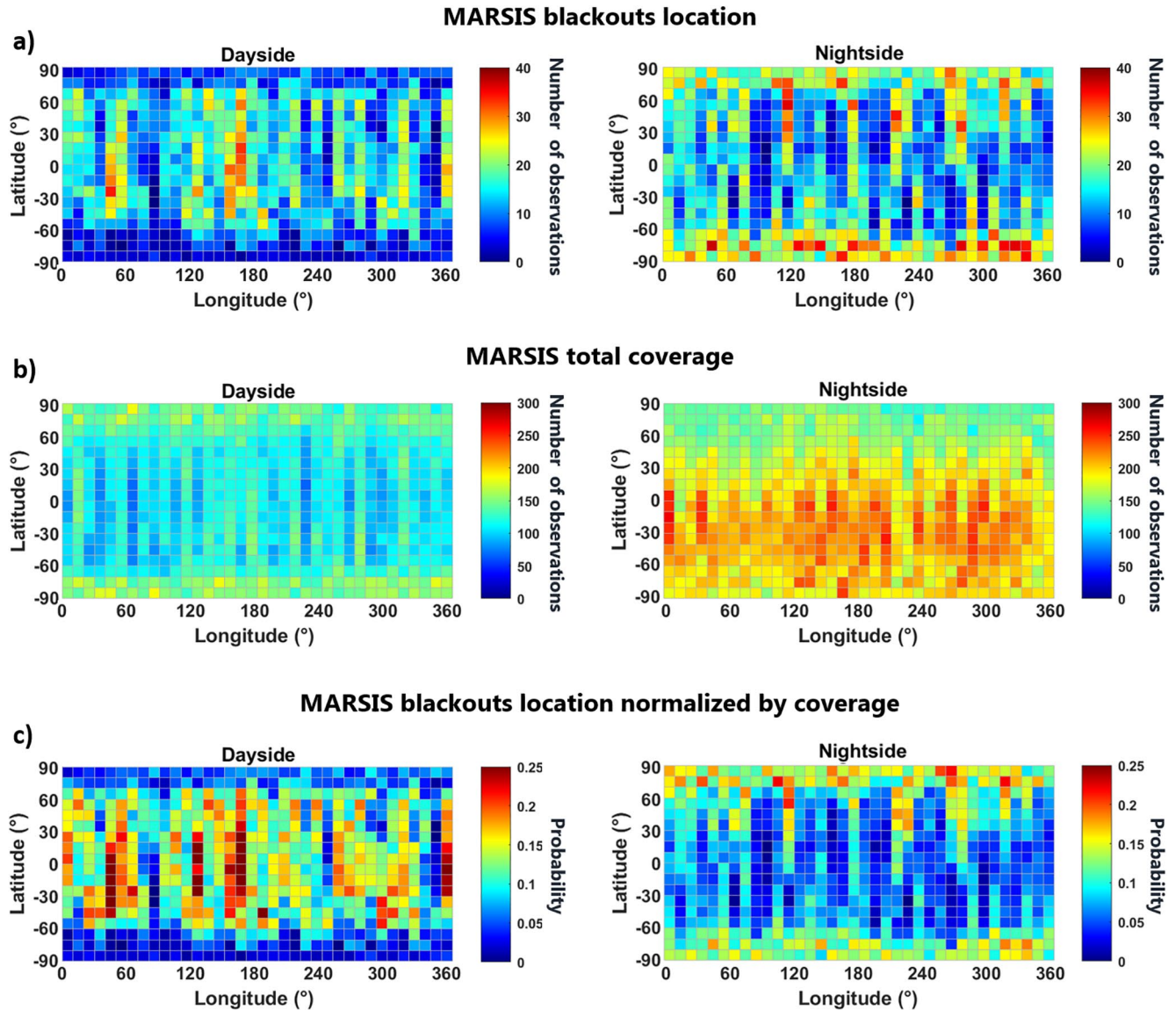
MARSIS blackouts location

MARSIS total coverage

MARSIS blackouts location normalized by coverage

Figure 3. The distribution of the occurrence of MARSIS radar blackouts as a function of Martian planetocentric coordinates, in the IAU reference frame. The left hand panels represent dayside and the right hand panels represent nightside, which are separated by the X coordinate in the Mars-centered Solar Orbital reference frame. The bins in latitude and longitude are 10° of size. Panel (a) presents the occurrence of the blackouts, panel (b) presents the orbital coverage during the whole period, and panel (c) presents the normalized occurrence of the blackouts. Note that a color blind friendly version is available at https://doi.org/10.25392/leicester.data.15097008.

nightside, the normalized occurrence frequency, or probability of a radar blackout, has the opposite distribution, with peaks at the polar latitudes and a smaller probability in the equatorial regions.

We follow this discussion by considering the occurrence of the radar blackouts as a function of SZA. Figure 4a presents the number of radar observations where there is a blackout, Figure 4b the total MARSIS coverage, and Figure 4c the normalized occurrence of the blackouts, or probability. The occurrence of a blackout does appear to peak close to the terminator on the dayside, at a SZA between 80° and 90°, with more events occurring overall when the SZA is less than 90°. However, we note that the coverage of the radar tends to peak for these values of SZA (Figure 4b), with relatively more observations on the dayside. This leads to a probability curve as a function of SZA with several interesting features (Figure 4c). First, there seems to be a steady decrease in probability as SZA increases, from 0.125 at 50° to 0.06 at 100°. The probability then increases, however, and peaks at 0.2 at a SZA of 150°, before decreasing again back to ∼0.1. It is important to note that the coverage and occurrence of events at the lowest and highest values of SZA are both relatively low. However, the decrease in the event
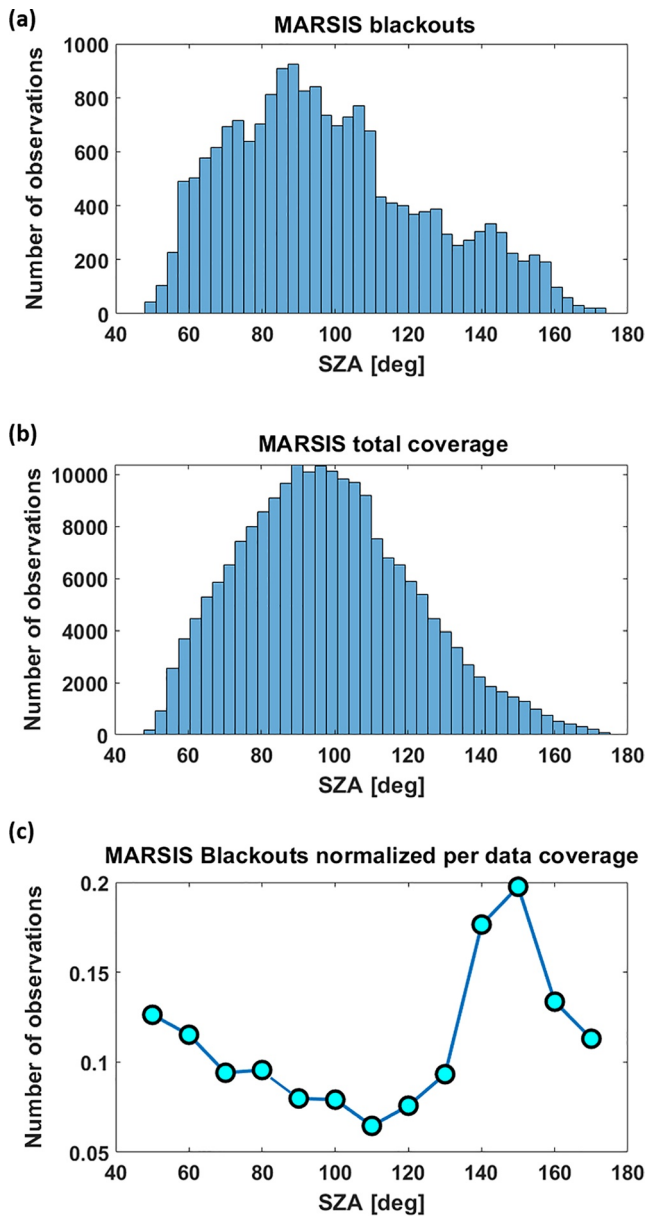
(a)

(b)

(c)

Figure 4. (a) Total number of MARSIS observations with blackouts per solar zenith angle (SZA). (b) Total number of MARSIS observations per SZA. (c) MARSIS blackout probability per SZA normalized by orbit coverage.

occurrence from about 60° onwards is certainly a real effect, while the secondary peak on the nightside is also real, although the subsequent decrease may be influenced by a result of the relatively small number of events.

The distribution of events does not follow the distribution of crustal magnetic fields (Acuña et al., 2001), where the crustal magnetic field strength is greatest in the southern hemisphere in the longitude sector 120° to 240° (Figure 3c). While there is a higher observed probability in this region on the dayside, there is a similar higher probability in northern latitudes where crustal fields are much weaker. Furthermore, on the nightside we note that the highest probability tends to be at the polar latitudes, with a higher probability again in the northern hemisphere.

Despite the relatively low number of orbits in certain locations, the intermittent operational nature of the MARSIS radar, and the intermittent nature of the solar wind causes of these blackouts, we conclude that the blackouts can occur over all parts of the planet with peak occurrence at different locations for dayside and nightside. Further, we note that there is an unexpected enhancement in radar blackout occurrence at SZA = 150°, that is, deep in the nightside.

3.3. Solar Cycle Variation of Radar Blackouts

Figure 2 hints at a solar cycle variability of the radar blackouts and we investigate this further in Figure 5. The top panel (Figure 5a) presents for context the sunspots number measured at Earth, and the second panel (Figure 5b) the solar irradiance at 30.5 nm at Mars, which is the wavelength most responsible for ionizing CO_2 (e.g., Sanchez-Cano et al., 2015, 2016). This has been calculated using the TIMED SEE instrument (Woods & Eparvier, 2006), which measures the irradiance at this wavelength at Earth. We have extrapolated the irradiance level to Mars assuming a simple $1/r^2$ decrease. We did not consider phase-shifting forward or back in time to account for the Mars-Sun-Earth angle because data were essentially averaged over one solar rotation. The eccentricity of the Martian orbit about the Sun, therefore, introduces a clear approximate 2-year modulation to the irradiance level. We note that at Mars, the irradiance level reaches a minimum in 2008 and then increases, partly as a result of moving to perihelion, and then partly as a result of the solar cycle, reaching a peak at the end of 2015. Following this peak in 2015, the irradiance decreases such that at the end of the interval of interest the irradiance level is much the same as in 2008.

Figure 5c presents the occurrence of both full radar blackouts (red curve) and partial blackouts (blue curve) observed by MARSIS as a function of solar cycle. Here the orbit-normalized occurrence is plotted with a 6-month cadence due to the relatively small numbers of events. Apart from the first

half of 2007, we note that the early part of the observations sees relatively low occurrence rates of total blackouts, which only starts to increase in the first half of 2011, from when the level remains approximately the same at between 0.1 and 0.15, before a reduction back to zero in the latter half of 2015. The minimum in the first half of 2013 is unexpected, although this does include a 1-month period when no observations were made as a result of an eclipse interval (Figure 2). We also note that there were relatively few observations in the latter half of 2015, which may be responsible for the abrupt reduction to zero at that time. The occurrence of the partial blackouts (Figure 5c, blue curve) has a similar solar cycle variation, although it is interesting to note that the highest level of partial blackouts is in the first half of 2007. While there is then a reduction in the occurrence of partial blackouts during the extended solar minimum (late 2007 to early 2010), during this time frame partial blackouts were more frequent than total blackouts.

Figure 5. The OMNI Sunspot number at Earth (panel a), the solar irradiance at Mars based on TIMED SEE data (panel b), the orbit-normalized occurrence of total (red line) and partial (blue line) blackouts on MARSIS (panel c), and the orbit-normalized occurrence of total (red line) and partial (blue line) blackouts on SHARAD (panel d).

Figure 5d presents the same normalized occurrence rate of full (red) and partial (blue) blackouts observed by SHARAD, wherein it is not until 2011 that any blackout, total or partial, is observed. After that, the highest level of total blackouts seen by SHARAD occurred in 2012. We also note that partial blackouts tend to be more frequent than total blackouts at SHARAD. The minimum in the first half of 2013 is also due to a lack of observations (Figure 2).
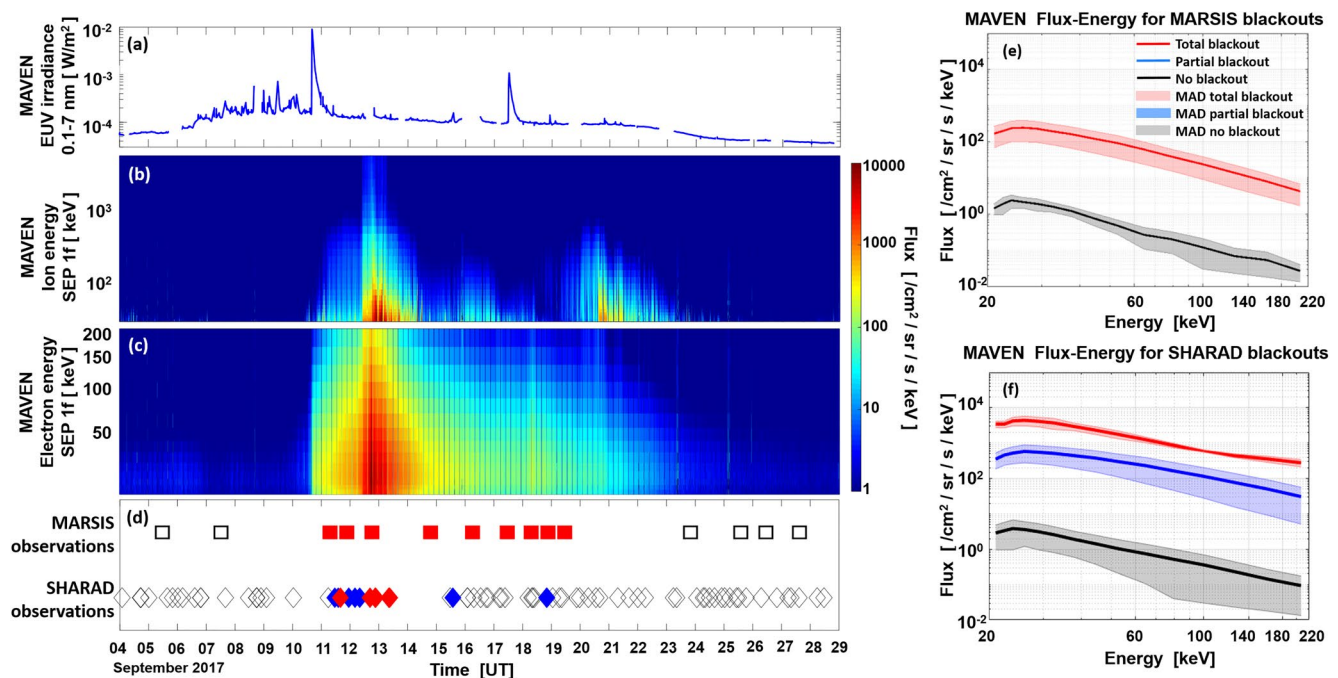
Figure 6. Case Study 1 (4 September to 29 September 2017). Panel a presents MAVEN EUVM irradiance observations. Panel b presents MAVEN SEP ion spectra. Panel c presents MAVEN Solar Energetic Particle SEP electron spectra. Panel d presents times of MARSIS (squares) and SHARAD (diamonds) operations. Red filled squares/diamonds represent a total blackout. Blue filled squares/diamonds represents a partial blackout. Panel e presents the median SEP electron energy flux curves for MARSIS (red curve for total blackouts, black curve for no blackouts). Panel f presents the median SEP electron energy flux curves for SHARAD (red curve for total blackouts, blue curve for partial blackouts, black curve for no blackouts). The shadow areas represent the median absolute deviation (MAD). Note that a color blind friendly version is available at https://doi.org/10.25392/leicester.data.15097008.

To summarize, there appears to be a clear solar cycle variation in the occurrence of total blackouts for both radars with most events peaking close to the peak of the cycle. However, there is an intriguing feature in the declining phase of the previous cycle 23 when more partial blackouts than total blackouts are observed even by MARSIS.

4. Investigation of the SEP Energy-Flux Spectra

A key element of the work presented by Sanchez-Cano et al. (2019) is the demonstration that during the event in September 2017 the energetic electrons measured by SEP were most likely responsible for creating the enhanced electron density layers at low altitude in the Martian atmosphere. It was the presence of these energetic electrons throughout the interval, together with the modeling of the impact of a sample energy-flux spectrum on the creation of the enhanced electron density layer that was a key to this conclusion. As a follow-on, we now investigate the SEP electron energy-flux spectra for a number of examples of radar blackouts where there is a mixture of total and partial blackouts, to determine the difference between the flux levels at different energies responsible for the two types of blackout. During these examples, MARSIS operations were always on the nightside, while the SHARAD operations occurred on both the dayside and nightside. Further, this allows us to investigate the difference between the spectra for the blackout periods on MARSIS and SHARAD. The following case studies include the two largest SEP events in the interval after the arrival of MAVEN, a smaller event, and two periods when SEP electron increases were present but no radar blackout occurred.

4.1. Case Study 1 (04–29 September 2017)

The first event (Figure 6) we discuss is the September 2017 event studied by Sanchez-Cano et al. (2019). In the top panel of Figure 6 we present the MAVEN EUVM irradiance for the interval 4 September to 29 September 2017. These data demonstrate that there were two distinct solar flares during this interval, on 10 and 17 September 2017. Prior to the first flare, the irradiance had been higher than for much of the interval and somewhat variable. Figure 6b presents the flux of SEP ions as a function of energy and Figure 6c the SEP electrons. Note

that the energy range for the ions is different from the electrons. The electrons rapidly increased just after the solar flare on 10 September 2017, while the ions showed a more gradual increase of flux with energy at the same time. This was followed by a rapid enhancement on the 12 September 2017, which is related to the passage of an ICME. The ion flux seemed to reduce to lower levels more quickly than the electrons, which remained relatively high until a secondary enhancement associated with the solar flare on 17 September 2017. The electrons then decayed while there was another enhancement in the ions on 21 September 2017.

In Figure 6d, the timing of the orbits where MARSIS (squares) and SHARAD (diamonds) made observations are given. Red-filled symbols represent a total blackout of the signal, while the blue-filled symbols represent partial blackouts of the radars. We see that MARSIS observed a total blackout of the surface reflection from the 11 September 2017 until the 20 September 2017. Unfortunately, there were gaps of several days without any MARSIS observations prior to and after these dates. However, no blackouts were observed on the two orbits on 5 and 7 September 2017 and then the four orbits on 23, 25, 26 and 27 September 2017, during which the level of energetic electrons was low. SHARAD, on the other hand, made a number of observations. There was a period from 11 September 2017–13 September 2017 when each orbit was either totally or partially blacked out. Of the two orbits on the 15 September 2017, the first was not affected but the second only had a partial blackout. There was then another partial blackout on the 18 September 2017.

Figure 6e presents SEP electron flux versus energy spectra for this interval. The red curve represents the median values of the fluxes for the energies sampled by MAVEN SEP for those times when MARSIS was in total blackout. We note here that only spectra when MAVEN was in the solar wind, or in the magnetosheath close to the solar wind for those cases in which MAVEN did not transit the solar wind, have been considered in this analysis. The light shaded red regions illustrate the median absolute deviation (MAD), which is a robust measure of the variability in flux at each energy band. The black line is the same median value for the interval 4–10 September 2017 and 24–29 September 2017. It is clear that the median flux value at each energy bin during the radar blackout periods was two orders of magnitude higher than the periods where the radar signal strength was more typical.

Figure 6f presents the results of the same analysis of the SEP electron data during the SHARAD observations, although here we have an additional blue line representing the median flux-energy spectrum for the partial blackouts. The flux values during the radar blackout orbits are three orders of magnitude higher than those when there was no blackout. This higher level of fluxes is to be expected from Figures 6c and 6d since the SHARAD total blackouts occurred during the period of high intensity flux. In addition, the partial blackouts for SHARAD occurred during periods where the flux-energy spectrum was some two orders of magnitude higher than the no blackout spectrum. The former is similar to the energy-flux level during the total blackout for MARSIS. We might expect that the flux levels should be higher for SHARAD blackout periods in order to create the level of ionization to absorb the high frequency signal of SHARAD (Equation 1).

4.2. Case Study 2 (22 February–15 March 2015)

Our second Case Study is from 22 February 2015 to 15 March 2015, an event which has also been studied previously (e.g., Duru et al., 2017; Jakosky et al., 2015). This case is interesting for a variety of reasons: (a) there were three separate SEP events; (b) the ion spectra often had higher fluxes at the lower energy range; and (c) there was a mix of responses in both MARSIS and SHARAD data. Figure 7 is in the same format as Figure 6. The irradiance in the 0.1–7 nm waveband is presented in Figure 7a. Here there are a number of rapid enhancements in the irradiance, which are solar flares, but for most of the interval, the irradiance returns to the background level after the flare.

Figures 7b and 7c present the ion and electron SEP fluxes as a function of energy and time, respectively. There are two clear enhancements in both SEP ions and electrons, on 27 February 2015 and 3 March 2015, while on 6 March 2015 there is a third enhancement in SEP electrons, which is not readily visible in the ion counts. There is a third enhancement in ions on 8 March 2015 at the same time as a short-lived enhancement in the electrons. Note that there is an increased level in the ions before the first of these, which started on the 25 February 2015 but this is not seen in the electron counts. In general, the ion fluxes, especially in the lower energy range below 100 keV, tend to be higher than the electron fluxes. The second enhancement is short lived in SEP electrons, lasting for less than 24 hr, but continues longer for the ions.
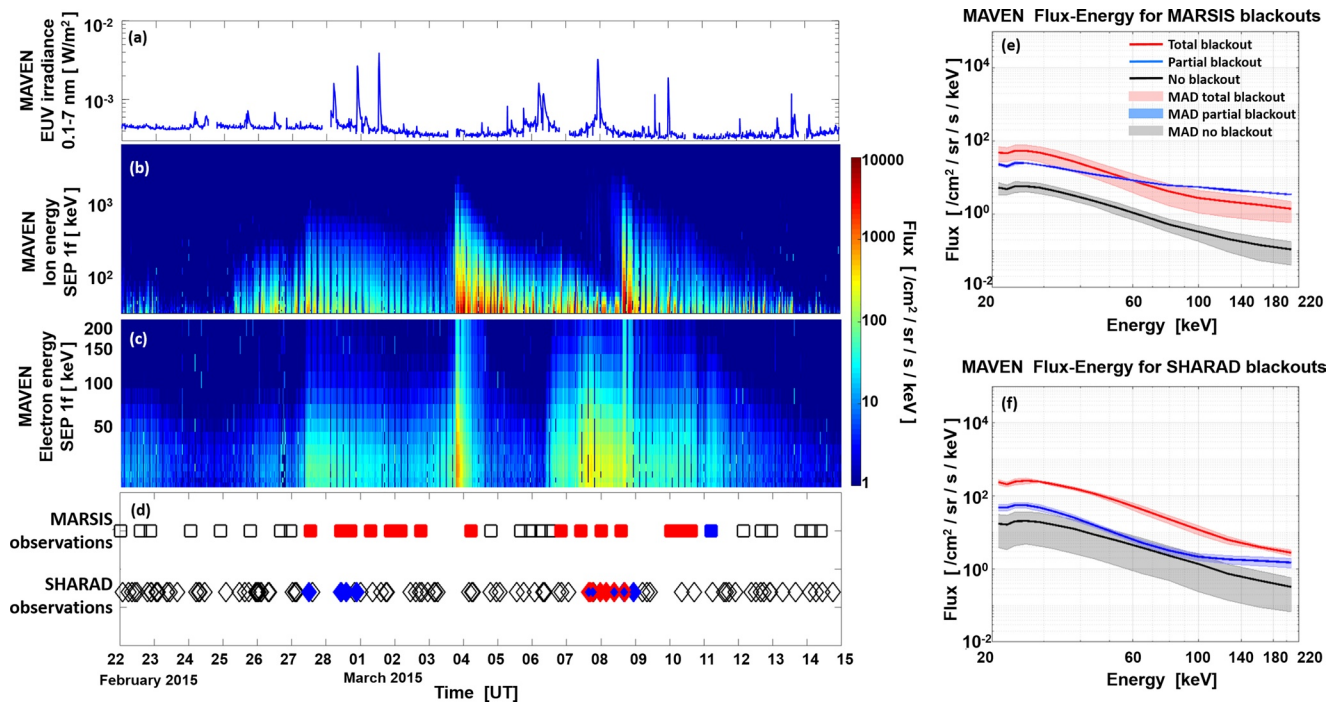
Figure 7. Case Study 2 (22 February to 15 March 2015). The format is the same as for Figure 6. Note that a color blind friendly version is available at https://doi.org/10.25392/leicester.data.15097008.

There were considerably more MARSIS orbits during this period than during Case Study 1. We note that MARSIS had its first total blackout immediately after the first enhancement in ions and electrons, but that prior to this when the ion fluxes were high at lower energies, the radar detected a reflected signal from the surface. This first blackout period at MARSIS lasted from 27 February 2015 until 4 March 2015, just after the second enhancement in the ion and electron fluxes. After this, there were five orbits during which there is no evidence of a blackout. This was the period when the electron fluxes were much lower than the ion fluxes (Figures 7b and 7c). After the third enhancement in electrons there was another period when MARSIS experienced blackout, from late on 6 March 2015 to late on 10 March 2015. This was followed by one partial blackout orbit on 11 March 2015, before returning to normal on 12 March 2015. We note here that the AIS observations during this interval also demonstrated that the surface reflection was at a much reduced signal level (Duru et al., 2017), with a slight increase in signal level during the time when no blackout was observed (4–6 March 2015).

SHARAD experienced partial blackouts only for a short period following the first enhancement in ions and electrons, from 27 February 2015 until late in 28 February 2015. The radar then continued to receive signals from the surface for all orbits until early on the 7 March 2015. Later that day there was a secondary enhancement in electrons, which resulted in SHARAD experiencing a mix of full and partial blackouts until late on the 8 March 2015. Thereafter the surface reflections returned to their more typical level.

Moving to the SEP flux energy spectra for the different periods of radar blackout, we see that the median spectrum for the total blackouts at MARSIS (Figure 7e) was again higher than when there was no blackout, but on this occasion only by an order of magnitude. We note, however, that the median spectrum for the orbits where no blackout occurred was higher than in Case Study 1. The flux from the one orbit where there was a partial blackout of MARSIS had a peak energy similar to the median spectra for the blackout periods and the non-blackout periods. This peak in energy occurs near 25 keV. However, there does seem to be a higher energy tail, such that the fluxes at energies above 60 keV were higher during this one partial blackout than during the median of the periods of the total blackout.

For SHARAD (Figure 7f), we note that the median spectrum for the non-blackout period was similar to that for MARSIS and again higher than in Case Study 1, but that for the total blackout observations the median spectrum had typically higher fluxes than for MARSIS under total blackout conditions. The median spectrum for the partial
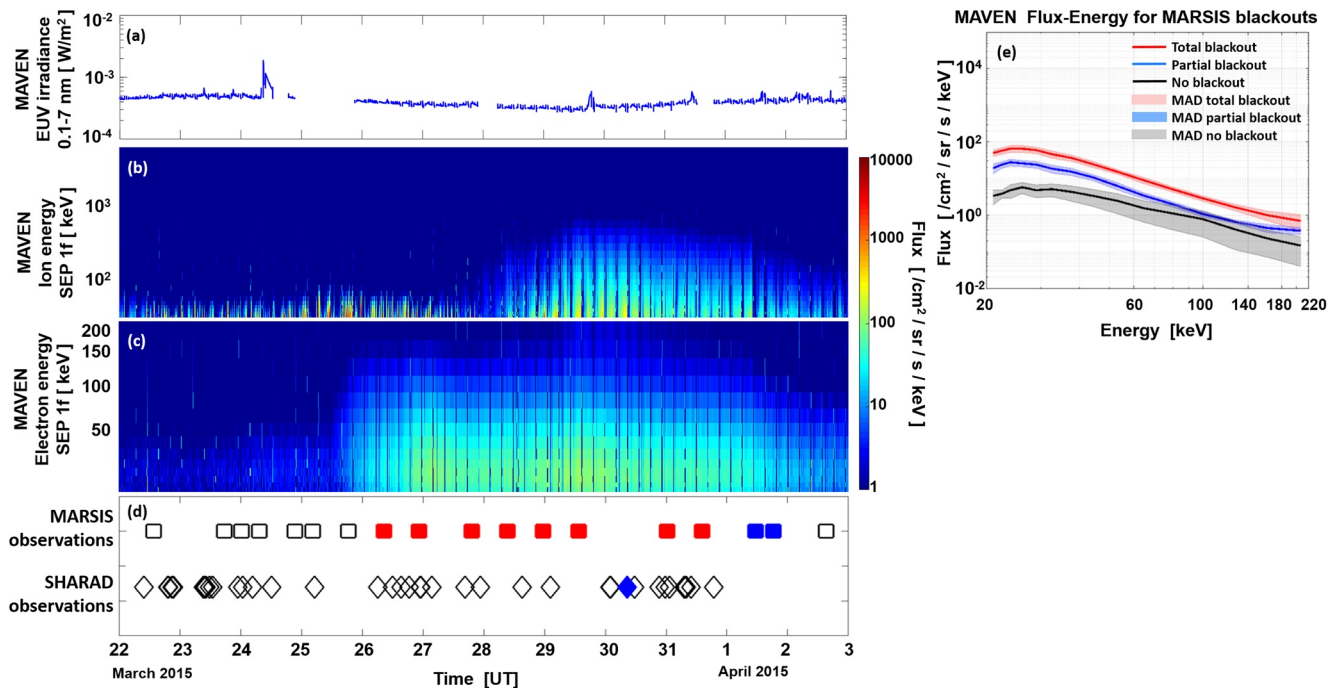
Figure 8. Case Study 3 (22 March to 3 April 2015). The format is the same as for Figure 6. Note that a color blind friendly version is available at https://doi.org/10.25392/leicester.data.15097008.

blackouts again lay between those for the total blackout and no blackout, but was much closer to the no blackout spectrum than for Case Study 1.

4.3. Case Study 3 (22 March–03 April 2015)

Our next Case Study discusses an interval that followed on from the previous one and has been selected as this is the only remaining event where there were both full and partial blackouts in MARSIS data, although there were neither for SHARAD. Although weaker than the previous two case studies, it is still one of the largest events during the period under investigation when MAVEN was in orbit around Mars. Figure 8 presents the data in the same format as Figures 6 and 7 for the interval 22 March to 3 April 2015. The irradiance in the 0.1–7 nm wavelength band shows a single solar flare early on the 24 March 2015 during this interval (Figure 8a), but apart from two very much weaker events, there is little variability. This is then followed first by an increase in SEP electrons (Figure 8c) late on 25 March 2015 and then a more gradual increase in SEP ions (Figure 8b) starting on 27 March 2015. A further increase in SEP electrons occurred at the time of this enhancement in the SEP ions. Thereafter there was a general decay in the SEP electrons and ions.

MARSIS experienced its first total blackout early on 26 March 2015 (Figure 8d), a few hours after the arrival of the SEP electrons. This was followed by seven further orbits experiencing a total blackout until late on 31 March 2015. There were then two orbits on 1 April 2015 when there was a partial blackout of the MARSIS radar echoes. SHARAD only had one orbit throughout this interval that was affected, early on 30 March 2015, when there was a partial blackout of the surface reflection signal.

In this case, we do not consider the electron flux-spectrum for the SHARAD orbits, but concentrate on the median spectra for the three blackout occurrences for MARSIS as before (Figure 8e). The median flux-energy spectrum for those orbits where there was no blackout had a similar level to that in Case Study 1. The median flux-energy spectrum for the total blackout orbits was again not as high as Case Study 1 and more in line with that in Case Study 2. On this occasion, the median spectrum for the partial blackouts was somewhat higher in fluxes than in Case Study 2, but was still between the other two median spectra.
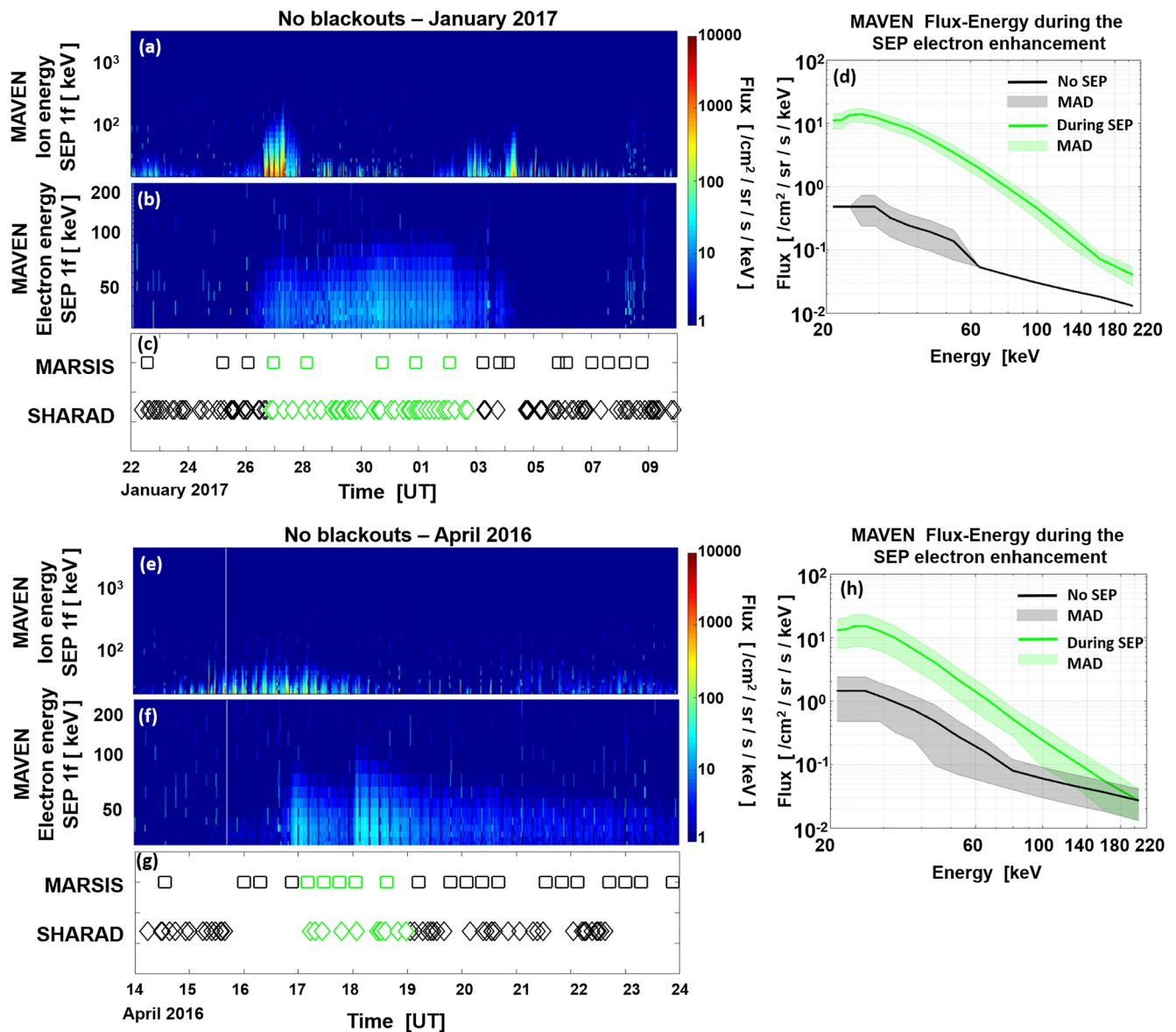
Figure 9. Case Study 4. Panels a to c present the Solar Energetic Particle (SEP) ion energy flux spectra, SEP electron energy flux spectra and the times of the orbits of MARSIS and SHARAD for the interval 22 January to 10 February 2017. Green squares/diamonds represent MARSIS/SHARAD orbits during high SEP electron fluxes. Panel d presents the median SEP electron energy flux spectra for the orbits identified by the green squares/diamonds in panel c and the black curve during the black squares/diamonds in panel c. Panel e to h present the same data but for the interval 14 April to 24 April 2016. Note that a color blind friendly version is available at https://doi.org/10.25392/leicester.data.15097008.

4.4. Case Study 4

Here we discuss two separate intervals, 22 January to 9 February 2017 and 14–24 April 2016. These two periods have increases in the SEP fluxes but no total or partial blackouts in either of the two radar data sets. The purpose of this Case Study is to investigate the SEP spectrum when such enhancements in SEP do not result in the blackout, either total or partial, of the radar signal. In panels a, b and c of Figure 9 the SEP ions, electrons, and the times of the MARSIS and SHARAD orbits, respectively, are plotted for the period 22 January to 10 February 2017. Panels e, f, and g of Figure 9 present the same data but for the 14–24 April 2016. In Figures 9a and 9b, we note an increase in the electrons and ions on 26 January 2017. The ions are initially relatively stronger at lower energies but short-lived, of order 24 hr, and followed by a series of smaller bursts over the next 8 days or so. The electrons on the other hand are more or less continuous for the interval 26 January to 2 February 2017, with a slight intensification occurring on 28 January 2017. The open squares and circles demonstrate that there were no total or partial blackouts for either
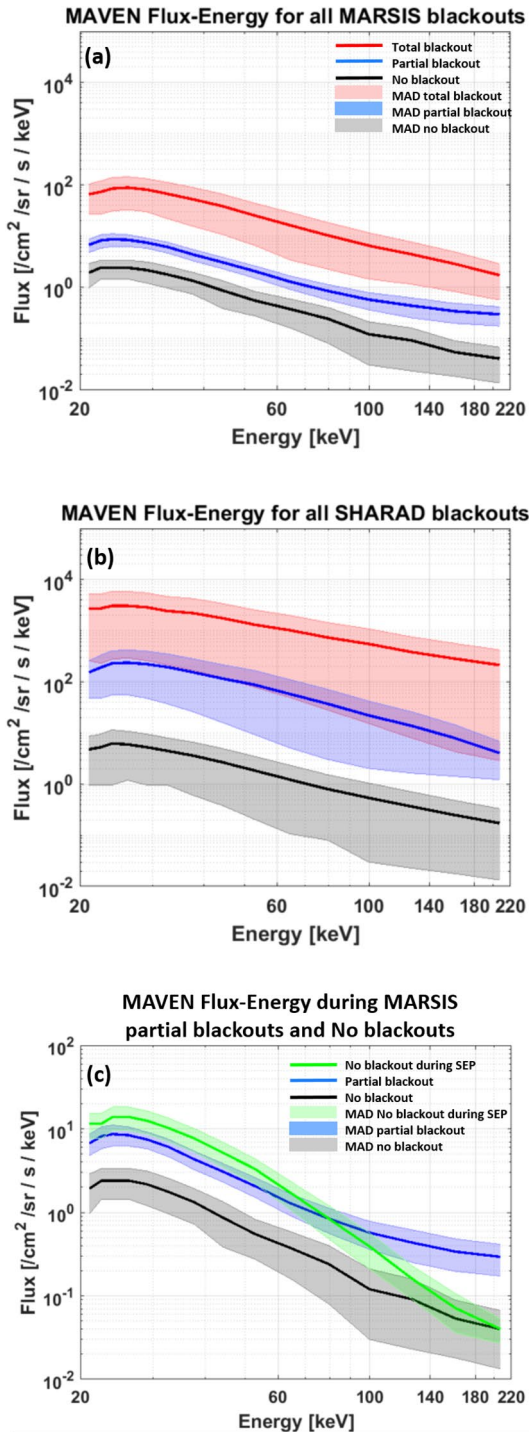
MAVEN Flux-Energy for all MARSIS blackouts

MAVEN Flux-Energy for all SHARAD blackouts

MAVEN Flux-Energy during MARSIS partial blackouts and No blackouts

Figure 10. (a) The median Solar Energetic Particle (SEP) electron energy flux spectra for the total blackouts (red curve), partial blackouts (blue curve) and no blackout for MARSIS during case studies 1–3. (b) The same representation but for the SHARAD orbits. (c) The green curve is the median SEP electron energy flux spectrum for the high SEP electron fluxes in Case Study 4 where there was no blackout. Note the different ordinate scale for panel (c) The blue curve is the same as the blue curve in panel a for partial blackouts at MARSIS and the black curve is the median SEP electron energy flux spectrum for the orbits where there was no blackout and low SEP electron fluxes (from Figure 9).

MARSIS or SHARAD observations. The green color indicates those orbits that occurred during the interval of the SEP electron enhancement. In Figure 9e, we see that the ions are relatively high at low levels for a period from 15 to 19 April 2016. The electrons on the other hand (Figure 9f) intensify on the 17 April 2016 and stay high for a 2-day period, with a second enhancement on 18 April 2016. Again, the open circles and squares in Figure 9g demonstrate we could find no evidence of a total or partial blackout during the period of enhanced electrons.

In Figure 9d, the green line presents the average spectrum for the orbits that occurred during the electron enhancements in the January/February 2017 interval while the black line is the average SEP electron spectrum for those without the enhancement. Similarly, Figure 9h presents the spectrum for the April 2016 interval. In the first case, we note that the energy flux during the non SEP orbits (black line) peaks at a lower level than previous similar average spectra during non-SEP orbits in the earlier case studies. In the second case, the energy flux during the non-SEP orbits is similar to those during orbits in the previous cases. In the January/February 2017 enhancement (Figure 9d) the average spectrum during the period of higher SEP (green curve) is at least an order of magnitude higher than the black curve at all energies. In the April 2016 enhancement (Figure 9h), the green curve is an order of magnitude higher than the black curve up to about 100 keV, and thereafter the two curves converge.

4.5. Summary of Case Studies

To summarize the results of the above case studies, we have considered a range of different responses of the radars to the presence of SEP electrons measured by MAVEN. However, to try to draw the observations together, in Figure 10 we replot the median spectra from the MAVEN SEP instrument for the electrons during the case studies discussed in this paper. Figure 10a presents the average SEP electron spectra for MARSIS, Figure 10b the central panel the average SEP electron spectra for SHARAD, and Figure 10c presents the average SEP electron spectra for the periods where SEP electrons were present but no blackout was recorded (green curve), based on the two events in the final Case Study. In each panel, the color coding follows that previously used for the spectra associated with the total, partial and no blackouts, that is, red, blue and black respectively. Key points to emerge are:

1. The median SEP electron energy-flux spectra for the orbits where there were total blackouts (red lines) of the MARSIS (Figure 10a) and SHARAD (Figure 10b) radars were typically higher than those where no blackout occurred (black lines) by at least an order of magnitude and often higher
2. The median SEP electron energy-flux spectrum where there were total blackouts at SHARAD (Figure 10b) was an order of magnitude higher than the median spectrum for MARSIS (Figure 10a) echoes that suffered a total blackout
3. The median SEP electron energy-flux spectrum for those orbits where there were partial blackouts (blue lines) typically occurred between the spectra where there was a total blackout and where there were no blackouts (Figures 10a and 10b)
4. The median SEP electron energy-flux spectrum for the SHARAD observations where there was a partial blackout (Figure 10b) has similar fluxes to the median spectrum of the MARSIS observations where there were total blackouts, and much higher fluxes than where partial blackouts occurred for MARSIS (Figure 10a)

5. The median SEP electron energy-flux spectrum for the events where SEP electrons were present but no blackout occurred is similar to the median spectrum for MARSIS partial blackouts (Figure 10c) at energies below 70 keV. At energies above 100 keV, the partial blackout flux is larger than the other two curves

5. Discussion

In the material above there are two separate strands to the analysis. In Section 3 we present a statistical analysis of when the radar blackouts occurred over a period of 11 years, the rate of occurrence of the events as a function of solar cycle, and finally where the radar blackouts were observed in relation to the surface of the planet, and hence the crustal magnetic fields. This was followed in Section 4 with a series of case studies where we have investigated the median flux-energy spectra of SEP electrons during total blackouts for both radars, partial blackouts for both radars and when there was no blackout. In this section we discuss these results in more detail.

5.1. Relationship of Radar Blackouts With Solar Cycle

Since the occurrence of the radar blackouts for MARSIS is much more frequent than for SHARAD, for example, Figure 2, we focus on the occurrence of the MARSIS blackouts. The solar cycle variation illustrated in Figure 5 demonstrates two important features. The first is that the occurrence of total blackouts maximizes between 2011 and 2016, which coincides with the period during the most active part of the solar cycle. Second, during the period 2006–2011, which coincides with the period during the least active part of the solar cycle, there were more partial blackouts than total blackouts.

The first part of 2013 is an outlier in the high level of occurrence during high solar activity. Inspection of Figure 2 demonstrates that during the first part of that year there was a period of over 1 month when there were no MARSIS observations. Due to the large solar longitude separation between Earth and Mars at that time it is not possible to determine how many solar SEP events may have been missed from Earth based observations. However, we can use Earth based indices to provide an overview of the level of activity and in particular the Disturbance Storm-time, *Dst* index, which was introduced specifically to provide a measure of magnetic storm activity at Earth (Sugiura & Kamei, 1991). In the first 6 months of 2013, *Dst* indicates few periods of magnetic storm activity, suggesting that the Sun may have been relatively quiet, despite being close to solar maximum. Further investigation of the Heliocast prediction catalog of Coronal Mass Ejection (CME) arrivals at Mars (https://helioforecast.space/arrcat) suggests that no events would have impacted on the planet during this time. It does seem likely, therefore, that the relatively low occurrence of total blackouts in this half-year period is a combination of the quiescent state of the Sun at that time and the lack of continuous observations.

Sanchez-Cano et al. (2019) demonstrated that the enhancement in the SEP electrons and ions they discussed was a result of a CME released following an *X*8.2 class flare on 10th September. The effects of this flare are clearly detectable in the irradiance observations at MAVEN (Figure 6). This space weather event has turned out to be one of the largest during MAVEN's period in orbit around Mars to date. If we then assume that the other radar blackouts are also related to similar (if weaker) space weather events, then the solar cycle variation of radar blackouts is to be expected, since such events are known to occur more often during the maximum phase of solar activity.

However, the interesting aspect is the number of partial blackouts during the minimum phase of the solar cycle is higher than the total blackouts (Figure 5). While this does not put the overall occurrence rate at the same level as during solar maximum, it does suggest that there may be a lower level of activity, or possibly a different type of event that results in apparently weaker effects at Mars. This will be discussed further when we address the SEP electron flux-energy spectra during the case studies.

5.2. Location and SZA Dependence of Radar Backouts

The presence of crustal magnetic fields with varying strength and direction over the surface of Mars provides an added complication in the study of solar wind-ionosphere-atmosphere coupling at Mars. The fields have been demonstrated to impact on the position of the magnetic pile up boundary (e.g., Edberg et al., 2008; Hall et al., 2016), as well as on the ionopause, when observed (Sanchez-Cano et al., 2020). Moreover, low suprathermal

electron "holes" have been seen to occur over regions of enhanced field (Hall et al., 2016). The observations presented in Figure 3 suggest that there is no significant relationship between the radar blackout occurrence and the location of the strongest crustal magnetic fields. The radar blackouts do occur over all parts of the surface of Mars. There does appear to be some evidence that might indicate that during the dayside there is a preferential region in the mid-latitudes in both hemispheres for radar blackouts to occur, while on the nightside, any preferred region appears to be the poles. The relatively few events, however, makes it difficult to conclude that this is the case.

In contrast, the SZA of the observations does appear to have an effect on the probability of occurrence of a blackout (Figure 4). While the total peak of blackout observations appears to peak close to the terminator, this location is clearly also the location of the peak in our observational coverage. Normalizing the number of blackouts gives the probability of the occurrence of blackouts, which as it turns out is smallest in the terminator region. The region where the probability is highest is deep in the nightside, just around 150°SZA. This discovery is interesting when considered with the different spatial locations on dayside and nightside discussed above. Taken together, this may be evidence of transport playing a role in the nightside events, although the most probable reason is electron precipitation from the Martian tail. Studies by DiBraccio et al., (2018)and Xu et al. (2020) have shown that Mars' tail is highly twisted, affecting the entire nightside region, and this twisting of the tail is mainly caused by the interaction of the crustal fields with the solar wind. Magnetic topology may, therefore, have an effect on the nightside ionosphere by allowing precipitation of electrons but not ions, and causing this increase in the blackout SZA dependence at 150°. Nevertheless, this is beyond the scope of this paper and will be properly investigated in a future study. We also note that during the daytime, the probability does decrease as the SZA increases, reaching a minimum just after the terminator at a SZA of about 100°. This implies that the background density of the peak electron density layer does not have a significant effect on the occurrence.

5.3. SEP Electron Flux-Energy Spectra

We now move to the discussion of the SEP electron flux-energy spectra during the total and partial blackouts. The key results were summarized in Section 4.5. We start our discussion with the average energy spectra during the total blackouts, which for the MARSIS orbits had a peak energy of order 25 keV and a peak flux of order 10^2 $cm^{-2}sr^{-1}s^{-1}kev^{-1}$, while for SHARAD observations the peak energy was also of order 25 keV, but a peak flux of 2×10^3 $cm^{-2}sr^{-1}s^{-1}kev^{-1}$. The flux during the SHARAD observations with a total blackout then decreased at a slightly slower rate with increasing energy compared with the MARSIS orbits during a total blackout.

The most likely cause for the loss of surface reflection is the absorption of the radio signal as it passes through the ionosphere (e.g., Duru et al., 2017; Sanchez-Cano et al., 2019). The absorption is proportional to the electron density at any given altitude and inversely proportional to the carrier frequency (see Equation 1). Hence, for the same electron density profile, the absorption of the MARSIS signal will be larger than that of the SHARAD signal, as the latter has a frequency, which is a factor of 4–5 higher. In addition, the absorption is proportional to the momentum-transfer electron-neutral collision frequency, ν. Because ν is itself proportional to the neutral density, n, which decreases with altitude, ν will also decrease with altitude. Thus, a small additional electron density at any altitudes lower than the main electron density peak will cause enhanced absorption, although the absorption is most effective at an altitude where the radar frequency is equal to ν.

In this paper, we have focused on SEP electrons producing the additional layer at lower altitudes. There are, however, three other potential sources of ionization that could be responsible. The first of these are the SEP ions, mainly protons, which accompany the SEP electrons. Sheel et al. (2012) modeled the effect of solar energetic protons observed at Earth on the Martian atmosphere to demonstrate that they can create additional ionization. Morgan et al. (2014) then suggested that the cause of the loss of AIS surface reflectivity during one of the early events identified in this study, in June 2011, was a result of energetic ions rather than electrons. Moreover, at Earth, similar absorption of HF radar signals can occur, with short lived events a result of the precipitation of auroral electrons. Longer lived events, that is, several days or more, similar to the events discussed here tend to be caused by energetic protons, at least in the first few days, rather than electrons (e.g., Rogers & Honary, 2015). We note, however, that while the fluxes of ions during our events are high in our three case studies, it is the electrons that are always present during the orbits where full or partial blackouts occur in both radars. Since there is no simple means of "storing" high energy protons similar to Earth's radiation belts due to the lack of an internal dipole magnetic field, we conclude that it is likely that the continuous presence of energetic electrons is a critical

factor. Furthermore, modeling of the September 2017 event (Sanchez-Cano et al., 2019) demonstrated that the electron fluxes could create a layer that provided sufficient absorption of both MARSIS and SHARAD signals. It is possible that the ions may still contribute to additional layers of ionization in the atmosphere of Mars and we will investigate this in a future paper.

A second alternative mechanism is the high fluxes of X-rays during the solar flares that are often a precursor to the SEPs. These tend, however, to be relatively short-lived and will only ionize the dayside atmosphere. The third alternative is ionization created during meteor showers. While this is a possibility that we have not investigated, such showers at Earth typically occur at specific times in the year and are related to the planet crossing the path of minor bodies (e.g., Lukianova et al., 2018). This suggests that there should be a 2-year periodic signature in our occurrence data that is not present in the observations (Figure 2). While it is certainly true that additional layers are created by meteoritic bombardment at Mars (e.g., Molina-Cuberos, et al., 2008) producing Mg^+ at similar altitudes as this study, recent studies using IUVS on MAVEN have questioned whether the ionization layers created by the meteors is as high as first thought (Crismani et al., 2017, 2019). We believe that such layers are not responsible for the absorption events discussed here, at least those after September 2014. The main reason is that they occur at the same time as solar wind SEP electrons at Mars, but also, because Sanchez-Cano et al. (2019) demonstrated that the absorption layers were made of O_2^+ instead of Mg^+, which was not found to increase by MAVEN-IUVS.

As demonstrated by Sanchez-Cano et al. (2019), who modeled the impact of a typical SEP electron spectrum from Case Study 1, such electrons do create an additional layer below the normal main ionospheric peak, centered around 90 km. Estimates of the absorption as a result of this layer are higher for the MARSIS frequency than the SHARAD frequency. Therefore, higher fluxes of SEP electrons would be expected to create a denser layer and/or a lower altitude layer depending on the exact energy spectrum, which would result in a higher attenuation rate or absorption level. In the case of the total blackouts, it is clear that the SEP electron spectrum during the SHARAD blackouts has higher fluxes at all energies, exactly as required from the above discussion. Moreover, the peak energy is similar in both the SHARAD and MARSIS cases, which suggests that the additional ionization is likely to be created at the same altitude.

Moving now to partial blackouts, we recall that they occur when the surface echo signal is either fully lost for only part of the orbit or is not entirely lost but is much reduced in amplitude. In the former case, the indication is that there is some structure associated with the creation of the additional electron density layer responsible for the absorption of the signal. This would suggest that the fluxes are insufficient to create the layer along the whole track of the observation. In cases when there is a greatly reduced return-signal from the surface we conclude that absorption is still present, but overall at a lower level. Such a lower level of attenuation would result from a reduction in the fluxes of the SEP electrons.

Figure 10b demonstrates that the median SEP electron energy flux spectrum for the SHARAD partial blackout orbits has lower flux levels at all energies than the median spectrum for the total blackouts. The shape of the spectrum, however, remains similar. On the other hand, comparison with the spectrum during the total blackouts of the MARSIS signal (Figure 10a) demonstrates similar flux levels at all energies for SHARAD's partial and MARSIS total blackouts. Finally, the median spectrum for partial blackout orbits for MARSIS has lower flux levels at all energies than the median spectrum for the total blackouts. These observations all confirm that the absorption is related to the energy flux levels as predicted through Equation 1.

It is also useful to compare the SEP electron flux-energy spectrum for MARSIS partial blackouts with that for the events where there was an enhancement in SEP, but no blackouts could be detected. The overall average for the latter is shown in Figure 10c, where it is compared with the partial blackouts spectrum from Figure 10a and the spectrum where there was no enhancement in SEP electrons. In general, the larger fluxes at higher energies are more effective in producing blackouts because they produce ionization at an altitude with higher values of neutral density, thereby increasing total attenuation. While the SEP electrons for periods of no blackouts have higher fluxes than the spectrum for the partial blackout orbits at low energies, it is at the higher energies where the partial blackout curve has enhanced fluxes. This is a critical point because it points to larger fluxes at higher energy being required for the partial blackout to occur, as these higher energies can penetrate deeper into the atmosphere, thereby creating enhanced ionization at higher values of the neutral density and thus increasing total attenuation.

Unfortunately, we are limited to events from September 2014 onwards for this part of the study. However, the results discussed above do have implications for the earlier orbits when there were no similar observations to those made with the MAVEN SEP instrument. The MAVEN SEP observations during the partial blackouts suggest that the larger number of partial blackouts during the solar minimum are likely a result of lower fluxes in the SEP energy range. The comparison of the partial blackout energy flux spectrum shown in Figure 10c also suggests that these partial blackouts would require a higher flux at the larger energies. Consequently, we infer that the partial blackouts are related to enhanced SEP events, but the energy spectrum has lower fluxes than required for a total blackout. This is an important conclusion because it does imply that radar blackouts at the MARSIS frequencies can occur at any time during the solar cycle, even if some of them are only partial.

Our observations also provide evidence for the impact of the SEP electrons on the lower ionosphere. The median flux levels measured here during total blackouts of the SHARAD echoes would become extremely intense, similar to the levels modeled in Sanchez-Cano et al. (2019). However, this does seem to be a maximum level, at least during the events we have been able to study from the MAVEN period. Lower fluxes are likely to create additional ionization but at lower magnitudes than during Case Study 1. Nevertheless, this additional ionization is sufficiently high to absorb the lower frequency MARSIS signal.

The radar blackouts can occur at any place above the surface of the planet, at least for SZA greater than 50°, suggesting that the lower ionosphere can become enhanced at any latitude and local time or SZA. MARSIS orbits often cover a wide range of latitudes during observations of total blackout. Moreover, the MAVEN observations are mostly taken at locations which differ from the locations of MEx and MRO. We also note that during Case Study 1, MAVEN observed global aurora during the period of the SEP electron enhancements, often at times close to the MARSIS and SHARAD orbits when total blackout was observed (Schneider et al., 2018). This indicates that the events we witness are probably a global phenomenon and the whole ionosphere is responding.

6. Summary and Conclusions

We present an analysis of radar surface echo blackouts observed by MARSIS on Mars Express and by SHARAD on the Mars Reconnaissance Orbiter for the interval 2006–2017. Such blackouts are caused by enhanced ionization at altitudes below 100 km resulting in increased absorption of the radar signals, which is very important for robotic and human exploration of Mars. Our main results are:

1. MARSIS suffered more blackouts than SHARAD due to its lower carrier frequency, as predicted by theory
2. There is a clear correlation of these events with the solar cycle
3. There is no apparent relationship between blackout occurrence and crustal magnetic fields
4. Blackouts tend to occur during both dayside and nightside observations of Mars, with different spatial distributions of occurrence
5. Blackouts have a peak occurrence probability on the nightside, at SZA of 150°
6. The average SEP spectrum that results in a blackout is particularly enhanced at the higher energy end of the spectrum, above an energy of about 70 keV
7. The median SEP electron energy-flux spectrum needed to create a total blackout at SHARAD frequencies is an order of magnitude higher than the median spectrum for MARSIS
8. The median SEP electron energy-flux spectrum for those observations with partial blackouts typically has flux levels between the spectra that creates a total blackout and the spectra for no blackouts
9. The median SEP electron energy-flux spectrum needed to create a partial blackout of SHARAD is equivalent to that needed to create a MARSIS total blackout

This study provides the first long-term characterization of the lower ionosphere of Mars, a region inaccessible to orbital and in situ observations. This characterization is essential for understanding the coupling of the lower and upper atmosphere under space weather activity, as well as how space weather affects HF radio propagation and HF communications through Mars' ionosphere. The observations demonstrate that during crewed exploration of Mars consideration of radio frequency usage in this frequency band, and possibly even higher, is essential.

Data Availability Statement

Mars Express MARSIS data set can be downloaded from the ESA Planetary Science Archive (https://www.cosmos.esa.int/web/psa/mars-express). Mars Reconnaissance Orbiter SHARAD data set as well as the MAVEN SEP and EUV datasets can be downloaded from the NASA Planetary Data System (https://pds-geosciences.wustl.edu/missions/mro/sharad.htm) and the MAVEN Science Data Center (https://pds-atmospheres.nmsu.edu/data_and_services/atmospheres_data/MAVEN/maven_main.html), respectively. The MARSIS and SHARAD blackout occurrence list can be downloaded from the University of Leicester figshare archive (https://doi.org/10.25392/leicester.data.15097008).

References

Acuña, M. H., Connerney, J. E. P., Wasilewski, P., Lin, R. P., Mitchell, D., Anderson, K. A., et al. (2001). Magnetic field of Mars: Summary of results from the aerobraking and mapping orbits. *Journal of Geophysical Research*, *106*(E10), 23403–23417. https://doi.org/10.1029/2000JE001404

Andrews, D. J., Barabash, S., Edberg, N., Gurnett, D., Hall, B., Holstrom, M., et al. (2016). Plasma observations during the Mars atmospheric "plume" event of March-April 2012. *Journal of Geophysical Research: Space Physics*, *121*, 3139–3154. https://doi.org/10.1002/2015JA022023

Campbell, B. A., Carter, L. M., Putzig, N. E., & Phillips, R. J. (2011). Autofocus correction of phase distortion effects on SHARAD echoes. *IEEE Geoscience and Remote Sensing Letters*, *99*, 939–942. https://doi.org/10.1109/lgrs.2011.2143692

Campbell, B. A., Putzig, N. E., Foss, F. J., & Phillips, R. J. (2014). SHARAD signal attenuation and delay offsets due to the Martian ionosphere. *IEEE Geoscience and Remote Sensing Letters*, *11*(3), 632–635. https://doi.org/10.1109/LGRS.2013.2273396

Campbell, B. A., & Watters, T. W. (2016). Phase compensation of MARSIS subsurface sounding data and estimation of ionospheric properties: New insights from SHARAD results. *Journal of Geophysical Research: Planets*, *121*, 180–193. https://doi.org/10.1002/2015JE004917

Cartacci, M., Amata, E., Cicchetti, A., Noschese, R., Giuppi, S., Langlais, B., et al. (2013). Mars ionosphere total electron content analysis from MARSIS subsurface data. *Icarus*, *223*(1), 423–437. https://doi.org/10.1016/j.icarus.2012.12.011

Cartacci, M., Sánchez-Cano, B., Orosei, R., Noschese, R., Cicchetti, A., Witasse, O., et al. (2018). Improved estimation of Mars ionosphere total electron content. *Icarus*, *299*, 396–410. https://doi.org/10.1016/j.icarus.2017.07.033

Chaffin, M. S., Chaufray, J. Y., Deighan, D., Schneider, N. M., Mayyasi, M., Clarke, J. T., et al. (2018). Mars H escape rates derived from MAVEN/IUVS Lyman alpha brightness measurements and their dependence on model assumptions. *Journal of Geophysical Research: Planets*, *123*, 2192–2210. https://doi.org/10.1029/2018JE005574

Chicarro, A., Martin, P., & Traunter, R. (2004). *Mars express: A European mission to the red PlanetSP-1240*. Eur. Space Agency Publ. Div. (pp. 3–16).

Conroy, P., Quinsac, G., Floury, N., Witasse, O., Cartacci, M., Orosei, R., & Sanchez-Cano, B., et al. (2020). A new method for determining the total electron content in Mars' ionosphere based on Mars Express MARSIS data. *Planetary and Space Science*, *182*, 104812. https://doi.org/10.1016/j.pss.2019.104812

Crismani, M. M. J., Deighan, J., Schneider, N. M., Plane, J. M. C., Withers, P., Halekas, J., et al. (2019). Localized ionization hypothesis for transient ionospheric layers. *Journal of Geophysical Research: Space Physics*, *124*, 4870–4880. https://doi.org/10.1029/2018JA026251

Crismani, M. M. J., Schneider, N. M., Plane, J. M. C., Evans, J. S., Jain, S. K., Chaffin, M. S., et al. (2017). Detection of a persistent meteoric metal layer in the Martian atmosphere. *Nature Geoscience*, *10*, 401–404. https://doi.org/10.1038/NGEO2958

DiBraccio, G. A., Luhmann, J. G., Curry, S. M., Espley, J. R., Xu, S., Mitchell, D. L., et al. (2018). The twisted configuration of the Martian magnetotail: MAVEN observations. *Geophysical Research Letters*, *45*, 4559–4568. https://doi.org/10.1029/2018GL077251

Duru, F., Gurnett, D. A., Morgan, D. D., Halekas, J., Frahm, R. A., Lundin, R., et al. (2017). Response of the Martian ionosphere to solar activity including SEPs and ICMEs in a two-week period starting on 25 February 2015. *Planetary and Space Science*, *145*, 28–37. https://doi.org/10.1016/j.pss.2017.07.010

Edberg, N. J. T., Lester, M., Cowley, S. W. H., & Eriksson, A. I. (2008). Statistical analysis of the location of the Martian magnetic pile-up boundary and bow shock and the influence of crustal magnetic fields. *Journal of Geophysical Research*, *113*, A08206. https://doi.org/10.1029/2008JA013096

Eparvier, F. G., Chamberlin, P. C., Woods, T. N., & Thiemann, E. M. B. (2015). The solar extreme ultraviolet monitor for MAVEN. *Space Science Reviews*, *195*(1-4), 293–301. https://doi.org/10.1007/s11214-015-0195-2

Espley, J. R., Farrell, W. M., Brain, D. A., Morgan, D. D., Canor, B., Plaut, J. J., et al. (2007). Absorption of MARSIS radar signals: Solar energetic particles and the dayside ionosphere. *Geophysical Research Letters*, *34*, L09101. https://doi.org/10.1029/2006GL028829

Hall, B. E. S., Lester, M., Nichols, J. D., Sánchez-Cano, B., Andrews, D. J., Opgenoorth, H. J., & Fränz, M. (2016). A survey of superthermal electron flux depressions, or "electron holes," within the illuminated Martian induced magnetosphere. *Journal of Geophysical Research: Space Physics*, *121*, 4835–4857. https://doi.org/10.1002/2015JA021866

Hall, B. E. S., Lester, M., Sánchez-Cano, B., Nichols, J. D., Andrews, D. J., Edberg, N. J. T., et al. (2016). Annual variations in the Martian bow shock location as observed by the Mars express mission. *Journal of Geophysical Research: Space Physics*, *121*(11), 11474–11494. https://doi.org/10.1002/2016JA023316

Jakosky, B. M., Brain, D., Chaffin, M., Curry, S., Deighan, J., Grebowsky, J., et al. (2018). Loss of the Martian atmosphere to space: Present-day loss rates determined from MAVEN observations and integrated loss through time. *Icarus*, *315*, 146–157. https://doi.org/10.1016/j.icarus.2018.05.030

Jakosky, B. M., Lin, R. P., Grebowsky, J. M., Luhmann, J. G., Mitchell, D. F., Beutelschies, G., et al. (2015). The Mars atmosphere and volatile evolution (MAVEN) mission. *Space Science Reviews*, *195*, 3–48. https://doi.org/10.1007/s11214-015-0139-x

Krishnaprasad, C., Smitha, V., Thampi, B. A., Christina, O., Lee, K., Kishore Kumar, K., & Pant, T. K.. (2020). Recurrent solar energetic particle flux enhancements observed near Earth and Mars. *Astrophysical Journal*, *902*, 13. https://doi.org/10.3847/1538-4357/abb137

Larson, D., Lillis, R. J., Lee, C. O., Dunn, P. A., Hatch, K., Robinson, M., et al. (2015). The MAVEN solar energetic particle investigation. *Space Science Reviews*, *175*, 153–172. https://doi.org/10.1007/s11214-015-0218-z

Lester, M., & Sanchez-Cano, B. (2021). *Radar blackouts at Mars*. University of Leicester. https://doi.org/10.25392/leicester.data.15097008

Lukianova, R., Kozlovsky, A., & Lester, M. (2018). Recognition of meteor showers from the heights of ionization trails. *Journal of Geophysical Research: Space Physics*, *123*, 7067–7076. https://doi.org/10.1029/2018JA025706

Molina-Cuberos, J. G., Lopez-Moreno, J. J., & Arnold, F. (2008). Meteoric layers in planetary atmospheres. *Space Science Reviews*, *137*, 175–191. https://doi.org/10.1007/s11214-008-9340-5

Montmessin, F., Korablev, O., Lefèvre, F., Bertaux, J. L., Fedorova, A., Trokhimovskiy, A., et al. (2017). SPICAM on Mars express: A 10 year in-depth survey of the Martian atmosphere. *Icarus*, *297*, 125–216. https://doi.org/10.1016/j.icarus.2017.06.022

Morgan, D. D., Dieval, C., Gurnett, D. A., et al. (2014). Effects of a strong ICME on the Martian ionosphere as detected by Mars express and Mars Odyssey. *Journal of Geophysical Research: Space Physics*, *119*, 5891–5908. https://doi.org/10.1002/2013JA0195222014

Morgan, D. D., Gurnett, D. A., Kirchner, D. L., Huff, R. L., Brain, D. A., Boynton, W. V., et al. (2006). Solar control of radar wave absorption by the Martian ionosphere. *Geophysical Research Letters*, *33*, L13202. https://doi.org/10.1029/2006GL026637

Nielsen, E., Morgan, D. D., Kirchner, D. L., Plaut, J. J., & Picardi, G. (2007). Absorption and reflection of radio waves in the Martian ionosphere. *Planetary and Space Science*, *55*, 864–870. https://doi.org/10.1016/j.pss.2006.10.005

Opgenoorth, H. J., Andrews, D. J., Fränz, M., Lester, M., Edberg, N. J. T., Morgan, D., et al. (2013). Mars ionospheric response to solar wind variability. *Journal of Geophysical Research: Space Physics*, *118*(10), 6558–6587. https://doi.org/10.1002/jgra.50537

Orosei, R., Jordan, R. L., Morgan, D. D., Cartacci, M., Cicchetti, A., Duru, F., et al. (2015). Mars advanced radar for subsurface and ionospheric sounding (MARSIS) after nine years of operation: A summary. *Planetary and Space Science*, *112*, 98–114. https://doi.org/10.1016/j.pss.2014.07.010

Picardi, G., Biccari, D., Seu, R., Plaut, J., Johnson, W. T. K., Jordan, R. L., et al. (2004). MARSIS: Mars advanced radar for subsurface and ionosphere sounding. In A. Wilson, & A. Chicarro (Eds.), *Mars Express: The scientific payload* (Vol. 1240, pp. 51–69). ESA Special Publication.

Rogers, N. C., & Honary, F. (2015). Assimilation of real-time riometer measurements into models of 30 MHz polar cap absorption. *Journal of Space Weather and Space Climate*, *5*, A8. https://doi.org/10.1051/swsc/2015009

Safaeinili, A., Kofman, W., Mouginot, J., Gim, Y., Herique, A., Ivanov, A. B., et al. (2007). Estimation of the total electron content of the Martian ionosphere using radar sounder surface echoes. *Geophysical Research Letters*, *34*, L23204. https://doi.org/10.1029/2007GL032154

Safaeinili, A., Kofman, W., Nouvel, J., Herique, A., & Jordan, R. L. (2003). Impact of Mars ionosphere on orbital radar sounder operation and data processing, Planet. *Space Science*, *51*, 505–515. https://doi.org/10.1016/s0032-0633(03)00048-5

Sánchez–Cano, B., Blelly, P.-L., Lester, M., Witasse, O., Cartacci, M., Orosei, R., et al. (2019). Origin of the extended Mars radar blackout of September 2017. *Journal of Geophysical Research: Space Physics*, *124*, 4556–4568. https://doi.org/10.1029/2018JA026403

Sanchez-Cano, B., Hall, B. E. S., Lester, M., Mays, M. L., Witasse, O., Ambrosi, R., et al. (2017). Mars plasma system response to solar wind disturbances during solar minimum. *Journal of Geophysical Research: Space Physics*, *121*, 6611–6634. https://doi.org/10.1002/2016JA023587

Sánchez-Cano, B., Lester, M., Witasse, O., Milan, S. E., Hall, B. E. S., Blelly, P.-L., et al. (2015). Evidence of scale height variations in the Martian ionosphere over the solar cycle. *Journal of Geophysical Research: Space Physics*, *120*, 913–1010. https://doi.org/10.1002/2015JA021949

Sánchez-Cano, B., Lester, M., Witasse, O., Milan, S. E., Hall, B. E. S., Cartacci, M., et al. (2016). Solar cycle variations in the ionosphere of Mars as seen by multiple Mars Express data sets. *Journal of GeophysicalResearch: Space Physics*, *121*, 2547–2568. https://doi.org/10.1002/2015JA022281

Sánchez-Cano, B., Morgan, D. D., Witasse, O., Radicella, S. M., Herraiz, M., Orosei, R., et al. (2015). Total electron content in the Martian atmosphere: A critical assessment of the Mars express MARSIS data sets. *Journal of Geophysical Research: Space Physics*, *120*, 2166–2182. https://doi.org/10.1002/2014JA020630

Sánchez-Cano, B., Narvaez, C., Lester, M., Mendillo, M., Mayyasi, M., Holmstrom, M., et al. (2020). Mars' ionopause: A matter of pressures. *Journal of Geophysical Research: Space Physics*, *125*, e2020JA028145. https://doi.org/10.1029/2020JA028145

Sá nchez-Lavega, A., Munoz, A. G., Garcia-Melendo, E., Perez-Hoyos, S., Gomez-Forrellad, J. M., Pellier, C., et al. (2015). An extremely high-altitude plume seen at Mars' morning terminator. *Nature*, *518*, 525–528.

Schneider, N. M., Jain, S. K., Deighan, J., Nasr, C. R., Brain, D. A., Larson, D., et al. (2018). Global aurora on Mars during the September 2017 space weather event. *Geophysical Research Letters*, *45*, 7391–7398. https://doi.org/10.1029/2018GL077772

Seu, R., Biccardi, D., Orosei, R., Lorenzoni, L. V., Phillips, R. J., Marinangeli, L., et al. (2004). SHARAD: The MRO 2005 shallow radar. *Planetary and Space Science*, *52*, 157–166. https://doi.org/10.1016/j.pss.2003.08.024

Sheel, V., Haider, S. A., Withers, P., Kozarev, K., Jun, I., Kang, S., et al. (2012). Numerical simulation of the effects of a solar energetic particle event on the ionosphere of Mars. *Journal of Geophysical Research*, *117*, A05312. https://doi.org/10.1029/2011JA017455

Stergiopoulou, K., Andrews, D. J., Edberg, N. J. T., Halekas, J., Kopf, A., Lester, M., et al. (2020). Mars express observations of cold plasma structures in the Martian magnetotail. *Journal of Geophysical Research: Space Physics*, *125*, e2020JA028056. https://doi.org/10.1029/2020JA028056

Sugiura, M., & Kamei, T. (1991). *Equatorial Dst index 1957 – 1986, IAGA bull., 40*. IUGG.

Witasse, O., Nouvel, J.-F., Lebreton, J.-P., & Kofman, W. (2001). HF radio wave attenuation due to a meteoric layer in the atmosphere of Mars. *Geophysical Research Letters*, *28*, 3039–3042. https://doi.org/10.1029/2001gl013164

Withers, P. (2011). Attenuation of radio signals by the ionosphere of Mars: Theoretical development and application to MARSIS observations. *Radio Science*, *46*, RS2004. https://doi.org/10.1029/2010RS004450

Woods, T. N., & Eparvier, F. G. (2006). Solar ultraviolet variability during the TIMED mission. *Advances in Space Research*, *37*(2), 219–224. https://doi.org/10.1016/j.asr.2004.10.006

Xu, S., Mitchell, D. L., Weber, T., Brain, D. A., Luhmann, J. G., Dong, C., et al. (2020). Characterizing Mars's magnetotail topology with respect to the upstream interplanetary magnetic fields. *Journal of Geophysical Research: Space Physics*, *125*, e2019JA027755. https://doi.org/10.1029/2019JA027755

Zurek, R. W., & Smrekar, S. E. (2007). An overview of the Mars Reconnaissance Orbiter (MRO) science mission. *Journal of Geophysical Research*, *112*, E05S01. https://doi.org/10.1029/2006JE002701